



Investigations of vibration cutting mechanisms of Ti6Al4V alloy

Zongtao Sun, Fei Shuang*, Wei Ma*

Institute of Mechanics, Chinese Academy of Sciences, Beijing 100190, China

ARTICLE INFO

Keywords:

Metal vibration cutting
Stability limit
Shear banding instability
Machine wavy surface
Orthogonal cutting process

ABSTRACT

This work involves systematical study of high-speed vibration cutting process of Ti6Al4V on numerical and theoretical aspects for the first time. In numerical simulations, the one-tool and double-tool cutting models are established based on the coupling Eulerian-Lagrangian (CEL) finite element (FE) method, to simulate forced vibration (FV) and self-excited vibration (SEV) cutting phenomena respectively. In theoretical analysis, linear perturbation method is used to analyze the critical condition of shear localized instability of chip material in the FV cutting process, and stability limits analysis is performed to study the tool vibration stability in the SEV cutting process, which consider coupled effects of wavy cutting thickness and periodic instability of shear bands. Different from vibration assisted machining in low-speed cutting, it is found FV with attainable frequency in industry promotes the evolution of shear bands, increase the cutting force and reduce the machined quality, whereas high-frequency FV can help improve the cutting process. On the other hand, SEV with smooth cutting thickness is found an effective strategy to weaken the evolution of shear bands and decrease cutting force in the high-speed cutting. The stability limit of SEV is related to the friction damping coefficient at the rack face, the penetration damping resistance, the ratio of the oscillation frequency of top wavy surface and the instability frequency of shear bands. These findings would help deepen the understanding towards the vibration effects in metal cutting and provide practical guidance to restrain and utilize vibration in the vibration assisted machining.

1. Introduction

The machining of metals is inevitably accompanied by the vibration of machine tool-workpiece system. At the beginning of the 20th century, F.W. Taylor [1], a famous American mechanical engineer, pointed out that vibration is the “most obscure and delicate of all problems facing the machinist”. From that time, both scientists and engineers have been considering the vibration in cutting as one of the most important machining challenges, and until now, it is still a popular research topic in academic and engineering fields.

Vibration in cutting results in a lot of detrimental effects, such as poor machining quality, tool wear and damage increasing, high production costs and so on, and thus it should be eliminated as much as possible. For this purpose, many studies on cutting vibration have been performed in the last century [2–4]. The early pioneering work on the vibration cutting process should owe to Taylor [1]. He performed extensive studies on metal machining and proposed the cutting force model with 3/4 power law. In addition, he observed the ductile work-material cracking ahead of the tool edge in the metal cutting. The other early groundbreaking work belong to Arnold [5] who studied the causes influencing the performance of machine tool and the mechanism of tool vibration in the cutting of steel, and found that the cutting forces are

a function of cutting speed. Usually, three types of mechanical vibrations can be generated due to the insufficient dynamic rigidity of the machining tool-workpiece system [6].

- i) *Free vibration* occurs when the static equilibrium state of mechanical system gets disturbed. The causes may be the collision between tool and workpiece in cutting, poor anti-vibration measures of lathe and so on. Presently, the mechanisms of the free vibration have been sufficiently understood and can be effectively alleviated and even eliminated.
- ii) *Forced vibration (FV)* occurs when external harmonic excitations exist. The inducing causes may be the artificially applied excitation and poor matching between parts in machine tool assemblies. Similarly, the disadvantageous effects of FV on cutting process can be effectively alleviated. Moreover, engineers have made use of FV to develop innovative processing, such as vibration assisted machining, to improve the machining quality [2].

Different from the conventional cutting processing, vibration assisted cutting deliberately sets the machine tool to vibrate with prescribed frequency, which has been extensively applied in the manufacturing industry [6]. Linear vibration cutting [7] and elliptical vibration cutting technologies [8], for example, have been exhibiting the superior machining performances over the conventional cutting. Applications of

* Corresponding authors.

E-mail addresses: shuangfei@imech.ac.cn (F. Shuang), watwm@imech.ac.cn (W. Ma).

vibration assisted machining show that the advantageous vibration can availably reduce cutting forces [9], increase tool life [10], enhance cutting stability [11], and improve surface finishing [12]. Especially, vibration assisted machining have been successfully applied to the precision machining of various difficult-to-cut materials, such as Ti6Al4V [13], Inconel 718 [14], tungsten carbide [15], ceramics [16] and so on. In the transverse vibration-assisted cutting [17] and the ultrasonic vibration cutting [18], the cutting forces and feed forces can be evidently reduced and the surface finish is effectively improved.

In the linear vibration cutting process, the tool edge unavoidably hits the clearance face which results in the generation of tensile stress at the flank face and the spalling of tool material. In the elliptical vibration cutting process, the vibration trajectory of tool tip is along an elliptical locus [19]. Thus, the lubrication condition between the tool and workpiece can be improved and the friction phenomenon on the rake face is reduced effectively. Moreover, the shear deformation of material in the primary shear zone (PSZ) is easier to occur to improve the material removal rate. Presently, this technology has been applied to ultra-precision machining of various difficult-to-cut materials [20–23]. Based on this technology, Suzuki et al. [24] proposed a unique micro/nano sculpturing method and further explored the possibilities of functional surface machining. Zhang et al. [25] predicted the transient cutting force theoretically and studied the influence of transient cut thickness and shear angle as well as transition friction behavior at the rake face. In low-frequency vibration cutting tests, they measured the transient cutting forces and demonstrated the validation of analytical results.

An important progress in the elliptical vibration cutting technology is the application of non-resonant elliptical vibrator. Since the trajectory of tool tip can be precisely controlled by a piezoelectric actuator, fabricating the micro/nano structures becomes possible [26,27]. Shamoto and Moriwaki [20] further developed this technology by using the vertical stacked vibrator. In the elliptical vibration cutting process in microscopic scale, it can evidently decrease the cutting forces, suppress the burr development and improve the machined surface integrity. Kim and Loh [28,29] and Brehl and Dow [30] developed parallel stacked piezoelectric vibrator for the micro/nano machining. Brehl et al. [31] and Brocato et al. [32] applied this technology to fabricate micro/nano structures with hard copper and stainless steel.

iii) *Self-excited vibration* (SEV) results from internal harmonic excitations of the tool-workpiece system, which generally include the friction between tool-workpiece, thermo-mechanical effects or cyclic shear banding instability and wavy cut thickness in metal cutting [3,4]. The SEV in the cutting force direction induced by the friction between tool-workpiece on the clearance face is called as *frictional chatter* [33]. In the high-speed cutting, the material in PSZ undergoes severe shear deformation with sharply rising temperature and high strain rate. Thus, the adiabatic shear banding instability takes place in PSZ, which is named as *thermo-mechanical chatter* [34]. When the mechanical vibrations in the directions of cutting force and ploughing force simultaneously exists and mutually correlates, *mode coupling chatter* [35,36] emerge as a more intractable problem.

Regenerative vibration, as a common form of SEV, can be caused by the friction on the rake face and the clearance surface, wavy chip thickness, shear angle oscillations and so on [37]. Particularly in the turning of metals, the machined wavy surface results in the changing chip thickness and cutting forces due to the phase difference of wavy surfaces between two consecutive turning revolutions. The regenerative vibration brings destructive effects to the machine tool and has become the dominant vibration mechanism influencing the metal cutting process [38–40]. Therefore, some pressing issues like how to effectively control and avoid the regenerative vibration occurrence, and how to further eliminate its effects on the metal cutting process, have been studied widely.

The regenerative vibration can induce unstable cutting process of metals, obvious deterioration of machining quality and serious dam-

age of tool material. Tobias and Fishwick [41] and Tlustý and Poláček [42] studied the stability of tool system in vibration cutting. The wavy cut thickness induces new fluctuations in cutting forces and in turn gives rise to the regenerative vibration in cutting. The stability limit analysis shows that, once the cut depth is larger than the stability limit, the amplitude of dynamic cutting forces increases rapidly and the cutting process becomes unstable. Meritt [43] presented stability conditions to predict cutting vibration stability in terms of the depth of cut and the chip width. Tlustý [44] showed that the chip width governs the cutting process stability and the regenerative chatter in turning process. The critical chip width depends on the dynamics of tool-workpiece system, cutting conditions and tool geometry. Mahnama and Movahhedy [45] investigated the effects of cutting conditions on the vibration cutting and revealed the variation of shear angle and stability limit with cutting speed. The thermomechanical model proposed by Moufki et al. [46] predicted the dynamic cutting forces and the stability limits of vibration cutting process. Furthermore, the vibration signals, surface roughness and chip morphology measured in turning experiments verified the validity of theoretical prediction. Turkes et al. [47] performed the linear stability analysis of vibration cutting with a single degree of freedom model by using oriented transfer function and tau decomposition form to Nyquist criteria. Kim and Lee [48] performed the stability analysis of tool system chatter with two degrees of freedom model and obtained the good agreement between the predicted stability limits in theory and results in experiments. The stability lobe curve obtained by Gao et al. [49] shows that the vibration effect on cutting stability presents in high-speed cutting process and that the ultrasonic vibration of tool increases the stability of vibration cutting process. The analysis of Vela-Martínez et al. [50] showed that the structural stiffness cubic term gives a better description of the nonlinear behavior of vibration cutting process, which is useful in restoring stability and further understanding the nonlinearity of regenerative chatter.

From the above reviews, we can see that the current studies focused on the effect of vibration phenomenon on the continuous chip formation in low-speed cutting process and rarely involved the serrated chip formation in high-speed cutting process. It is well known that the periodic shear banding instability not only results in poor machining quality but also in severe wear of machine tool. Moreover, the shear banding instability acting as an extra source inducing the tool system vibration, makes the vibration cutting problem more complicated. Recently, a lot of researchers have shown that the vibration assisted machining technology can effectively improve the machining quality [2,8,13,14]. However, the existing studies rarely take into consideration the stability of chip flow in vibration cutting process. For example, how does the tool vibration influence the chip formation mechanism in the FV cutting process? How do the periodic shear banding instability and machined wavy surface oscillation affect the SEV cutting process and the stability limit of tool system? The solutions to these questions will be conducive to the further improvement of machining processing. Therefore, it is necessary to carry out in-depth study on the vibration cutting process.

From the viewpoint of numerical simulation, cutting process has been a classical difficult problem for a long time. In the cutting process of metals, work material first separates at the tool edge, and then the chip and machined workpiece move along the tool rake face and the cutting direction respectively. The separation trajectory between chip and workpiece can be preset, which make it convenient to simulate the cutting process. Various numerical methods have been established to model the metal cutting process, e.g. the arbitrary Lagrangian-Eulerian method, remeshing FE method, meshless FE method and material point method and so on. Although these methods are very successful in simulating conventional metal cutting process, some inextricable problems arise in the vibration cutting due to unknown separation trajectory between chip and workpiece and the severe mesh distortion with the large plastic deformation of work-material. To overcome these problems, Coupling Eulerian-Lagrangian (CEL) FE model was proposed by Shuang et al. [51], and show more natural advantages than conventional FE

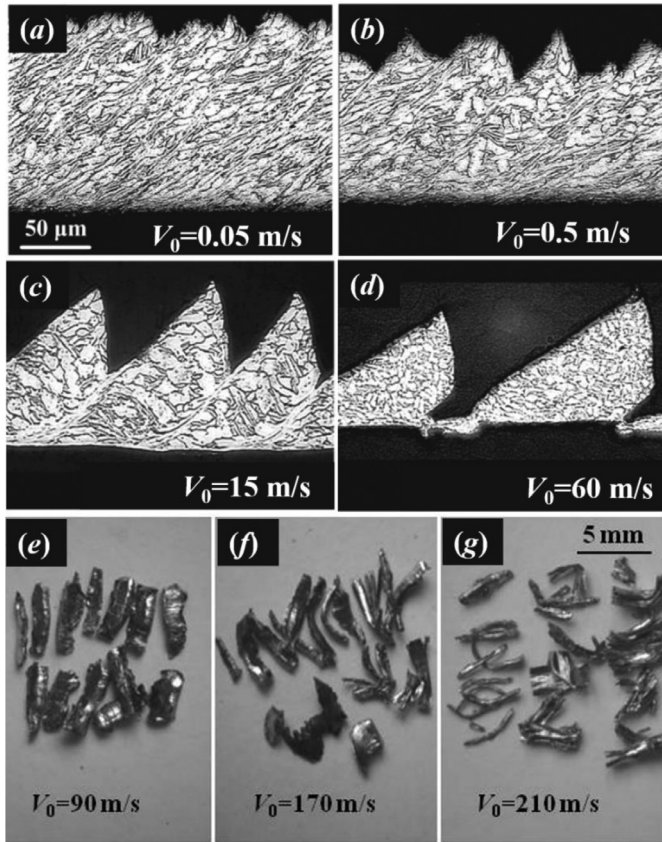


Fig. 1. The chip shape of Ti6Al4V alloy obtained in orthogonal cutting process.

methods in the simulation of vibration cutting process, which constitutes the foundation for the numerical analysis of vibration cutting mechanism in this paper.

The high-speed cutting mechanism of Ti6Al4V alloy has been studied in the orthogonal cutting experiments with a wide range of cutting speeds by Ma et al. [52] and Ye et al. [53]. The experimental results (Fig. 1) demonstrate that the chip shape varies with the increasing cutting speed from the continuous to serrated and then to debris with gradually decreasing thickness. Recent simulations showed that the serrated chip turns back to the continuous chip once the cutting speed approaches 300 m/s [54,55], which means that suppressing the occurrence of periodic shear banding instability is possible in the high-speed cutting processing to improve the machining quality. However, the cutting speed 300 m/s is unpractically high for tuning processing. The studies on the vibration cutting process [2,9] showed that the tool vibration in a specific frequency range can evidently improve the machining quality, whereas the mechanism is not understood completely for now. The interplay between periodic shear banding instability and different types of vibration, therefore, is our interest in this paper. Specifically, the numerical simulations of high-speed cutting of Ti6Al4V alloy with FV and SEV are carried out for the first time. Then, the theoretical analysis on the chip flow stability and the stability limit of tool vibration are performed. The influence of FV on the transition of chip shape and the influence of the shear banding instability on the stability limit of SEV in high-speed cutting process are investigated.

The intention of this work is threefold: (i) to provide an effective simulation method for studying the vibration cutting process of metals, (ii) to reveal the interplay between the periodic shear banding instability and the vibration cutting process, and (iii) to provide practical guidance to retrain and utilize vibration in the high-speed cutting process.

2. Numerical model

2.1. Coupling Eulerian-Lagrangian finite element model

Fig. 2a shows the CEL model for the numerical simulation of metal orthogonal cutting process. In this model, Lagrangian mesh is attached to the tool and Eulerian mesh is fixed in spatial. The latter is used to describe the motions and deformations of workpiece and chip materials. Moreover, the air mesh provides a sufficient large room for the growth of chips. In the simulation of metal cutting, the tool is fixed and the workpiece is constrained to move in negative x -axial direction. The boundary conditions with a constant horizontal cutting speed and zero vertical speed are imposed on the outer surfaces of workpiece. The uncut work-material flows into the Eulerian mesh region from the right boundary and the cut workpiece base flows out from the left boundary. The generated chips enter into the air mesh area. The unconstrained flow of chip on the free boundary is controlled by the volume approach of solid [56], which ensures chips to evolve as various shapes. Since the CEL model has, to a large extent, eliminated the influence of the mesh distortion and the limitation of the preset separation line method in Lagrangian FE method, it is convenient in the numerical simulation of vibration cutting process of metals with the unknown separation trajectory. In this model, the tool is idealized as rigid body with ideal sharp edge and infinite elastic modulus. The cutting conditions are prescribed by the cutting speed, cut thickness and the rake angle or the shear angle.

The Eulerian-Lagrangian contact algorithm is used [57] to describe the interaction between the tool and chips, which has been implanted into ABAQUS package. In order to focus on the vibration effect on cutting process, the friction contact at tool-chip interface is simplified to follow the Coulomb law with a constant friction coefficient even though the friction coefficient is related to the temperature and/or cutting speed [58]. The dynamic coupled thermo-mechanical analysis is performed in the simulation of metal cutting. For each time step, the heat and mass convection, heat conduction and stress are analyzed simultaneously. The workpiece and air mesh areas use the 8-node coupling thermo-mechanical linear Eulerian brick element EC3D8RT with reduced integration and hourglass control. The tool is described by the Lagrangian element C3D8RT. The simulation is carried out with commercial ABAQUS/Explicit package. For the detailed description of the CEL model, readers can refer to the article [51].

2.2. Material model

The work-material of Ti6Al4V alloy is assumed to be isotropic and thermo-viscoplastic. The Johnson-Cook (J-C) law was used to describe the plastic flow of Ti6Al4V alloy in cutting [18], which has the form

$$\sigma_{eq}^p = \left[A_0 + B_0 (\epsilon_{eq}^p)^n \right] \left(1 + C_0 \ln \frac{\dot{\epsilon}_{eq}^p}{\dot{\epsilon}_0} \right) \left[1 - \left(\frac{T - T_0}{T_m - T_0} \right)^m \right] \quad (1)$$

where σ_{eq}^p is the equivalent stress, ϵ_{eq}^p the equivalent plastic strain, $\dot{\epsilon}_{eq}^p$ the plastic strain rate, $\dot{\epsilon}_0$ the reference strain rate. T is the current temperature, T_0 the room temperature, T_m the melting temperature. A_0 , B_0 , C_0 , m and n are J-C constitution parameters. This constitutive model considers the effects of strain hardening, rate sensitivity and thermal softening on plastic flow of work-material. Material failure due to internal damage always has been incorporated in the simulations of chip formation in terms of the J-C fracture mode. The plastic flow of work-material is governed by J_2 flow-law. The material properties and constitutive parameters of Ti6Al4V alloy is given in Table 1 [59].

3. Forced-vibration cutting process

3.1. Shear bands frequency in orthogonal cutting

In the high-speed cutting of metals, the periodic shear banding instability of chip materials not only reduces the lifetime of tool, but also

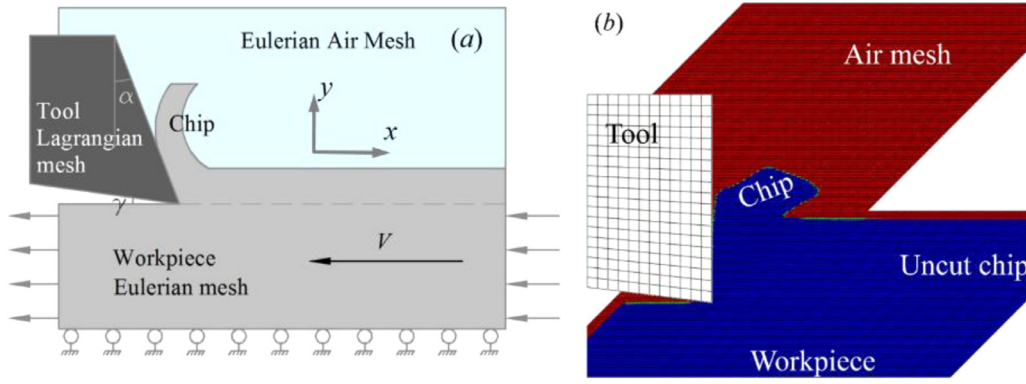


Fig. 2. (a) The CEL model for modeling the metal cutting process and (b) the FE mesh arrangement of this model.

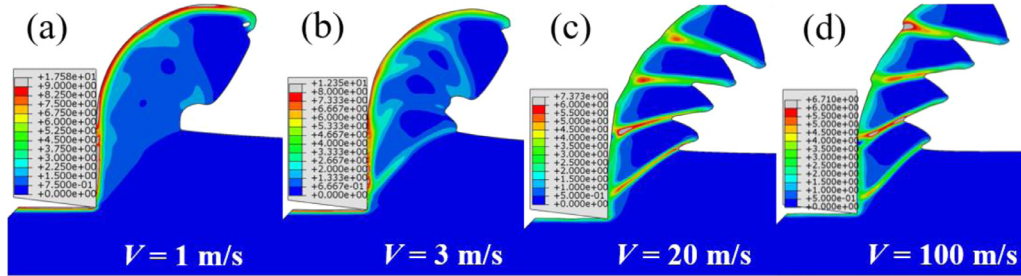


Fig. 3. Changes of chip morphology in convention cutting process with increasing cutting speeds.

Table 1
Material properties and constitutive parameter of Ti6Al4V and tool [59].

Properties symbol (Unit)	Ti6Al4V alloy workpiece	Tool
Density ρ (kg/m ³)	4430	11,900
Elastic modulus E (GPa)	114	630
Poisson's ratio ν	0.342	0.26
Specific heat c (J/kg·K)	520	334
Thermal conductivity λ (W/m·K)	6.7	100
Expansion coefficient α (K ⁻¹)	9.2×10^{-6}	5.4×10^{-6}
Melting temperature T_m (K)	1873	-
Fraction	0.9	-
Friction coefficient μ	0.4	-
Material parameters symbol (Unit)	Values	
A_0 (MPa)	725	
B_0 (MPa)	683	
n	0.47	
C_0	0.035	
m	1	
$\dot{\epsilon}_0$	10^{-3}	

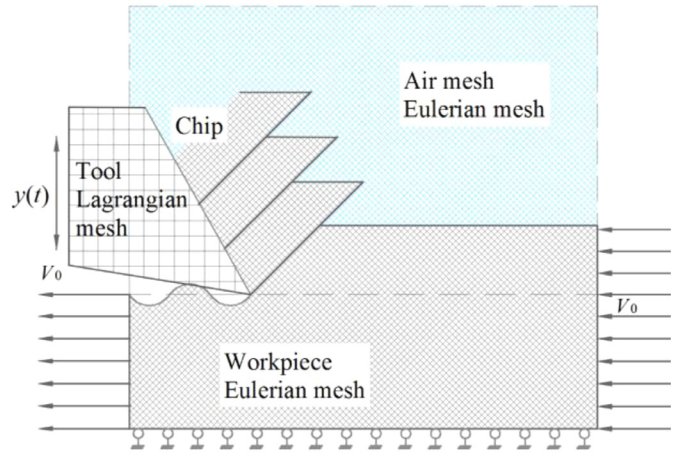


Fig. 4. The orthogonal cutting CEL FE model and the mesh arrangement.

deteriorates the machining quality of workpiece surface due to the tool vibration. The simulation results on the conventional cutting process of Ti6Al4V alloy (Fig. 3) shows that, when the cutting speed equals 3 m/s, the continuous chip turns into the serrated chip, which is close to the predicted results of Miguélez et al. [13]. As the cutting speed exceeds 3 m/s, the periodic shear banding instability occurs and leads to the formation of serrated chip. The previous study of [60] showed that the instability frequency of periodic shear bands f_{SB} is the important influence factor on the cutting process and can be determined through the FE simulation. Based on the total cutting time t_c and the number of shear bands N_{SB} (Fig. 3c and d), it can be defined as

$$f_{SB} = \frac{N_{SB}}{t_c} \quad (2)$$

In the vibration cutting process, the tool vibration changes the plastic flow stability of serrated chip, and conversely, the periodic shear band-

ing instability affects the vibration motion of tool system. The former as the FV cutting process will be considered in this section. The latter as the SEV process of tool will be studied in the next section.

3.2. Forced-vibration cutting simulation

For studying the FV cutting process, a single-free degree model is proposed to simulate the orthogonal cutting process of Ti6Al4V alloy. Fig. 4 demonstrates the model and the FE mesh arrangement in which the tool is modeled by the Lagrangian elements with material mesh whereas the plastic flow of the chip and workpiece material is described by the Eulerian elements with spatial mesh. The size of Eulerian mesh is set as 3 μm and the inclination angle is 45° relative to the horizontal direction. The cutting conditions are given as the cut thickness 100 μm , rake angle 0° and the cutting speeds 3 m/s, 20 m/s and 100 m/s. The tool vibration with a prescribed frequency is set in y-axial direction according

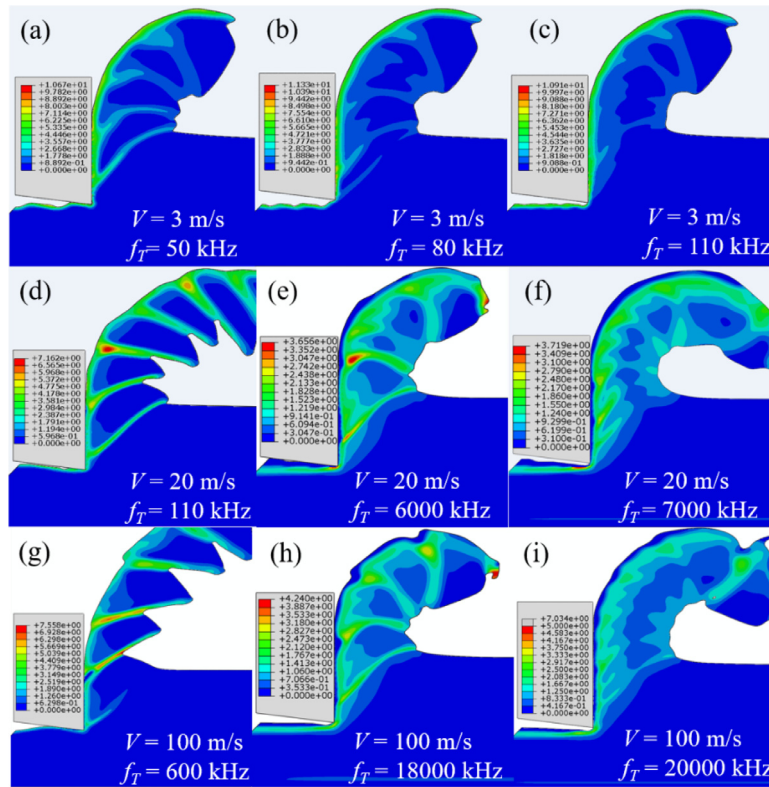


Fig. 5. The contours of equivalent strains obtained in the FV cutting processes with different FV frequencies of tool system and different cutting speeds ($V = 3, 20, 100$ m/s).

to a definite sinusoidal function $y(t) = A_0 \sin f_T t$, where $A_0 = 10 \mu\text{m}$ is the amplitude and f_T is the FV frequency of tool.

A wide range of frequencies are applied in simulations to study the FV cutting process, and the contours of equivalent strains are shown in Fig. 5. Compared with the simulation results of the conventional cutting process in Fig. 3, in the cutting process of 3 m/s, the low-frequency vibration of tool promotes the evolution of the shear bands, which make the continuous chip in the conventional cutting (Fig. 3b) transform into the serrated chip (Fig. 5a). However, as the FV frequency increases, the tool vibration tends to hinder the evolution of shear bands and results in the formation of continuous chip (Fig. 5b and 5c). In the high-speed cutting processes with 20 m/s and 100 m/s, the low-frequency FV promotes the evolution of shear bands in the serrated chip. Especially, when the FV frequency of tool equals the instability frequency of multiple shear bands, resonance occurs, which consumedly promotes the evolution of shear bands in the serrated chip (Fig. 5d and g). However, when the FV frequency is sufficient high, FV can completely suppress the nucleation and evolution of shear bands and makes the serrated chips (Fig. 3c and d) turn back into the continuous chips (Fig. 5e, f, h and i). Therefore, in the high-speed cutting process, there must exist a critical FV frequency f_{Tc} denoting the transition from the serrated chip to the continuous chip. Thus, as $f_T < f_{Tc}$, the periodic shear banding instability occurs in the serrated chip and the chip plastic flow is unstable; otherwise, when $f_T > f_{Tc}$, the continuous chip develops and the plastic flow of chip material becomes stable.

A serial of simulations are performed to calculate the transition FV frequencies under different cutting speeds and the results are illustrated in Fig. 6. The relation of instability frequency of the periodic shear bands with the cutting speed is also depicted in this figure. The two frequencies increase with the cutting speed according to a linearly proportional relationship. For the traditional cutting process, any point on the graphic plane would correspond to a serrated chip formation as the cutting speed exceeds the critical transition speed. However, in the FV cutting process,

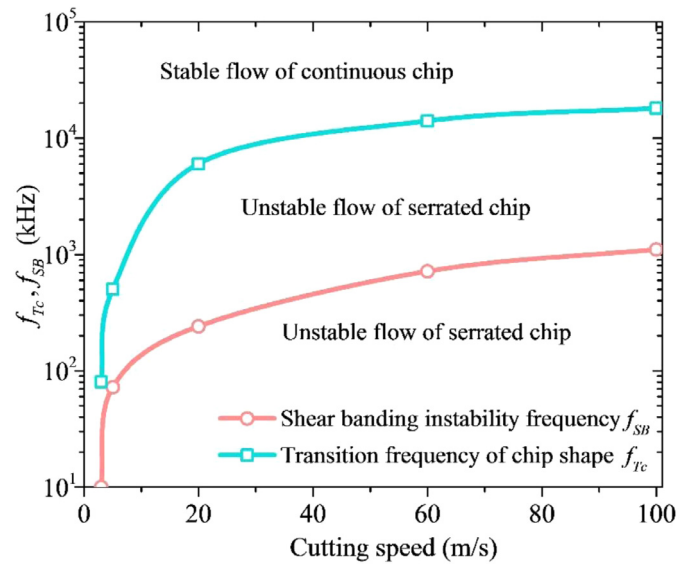


Fig. 6. The frequency of the shear banding instability f_{SB} and the FV frequency of tool at the transition of chip shape f_T vary with the cutting speeds.

these points with the higher FV frequency than f_{Tc} correspond to the continuous chip formation. Therefore, in the metal cutting process, applying a high-frequency FV to the tool system can obviously increase the plastic flow stability of chip material and improve the machining quality and processing efficiency. On the other hand, since the commonly used frequency in vibration assisted machining is usually less than 40 kHz [30], at which FV may promote the evolution of shear bands and causes more damage on tool life and machining quality. If a sufficiently high

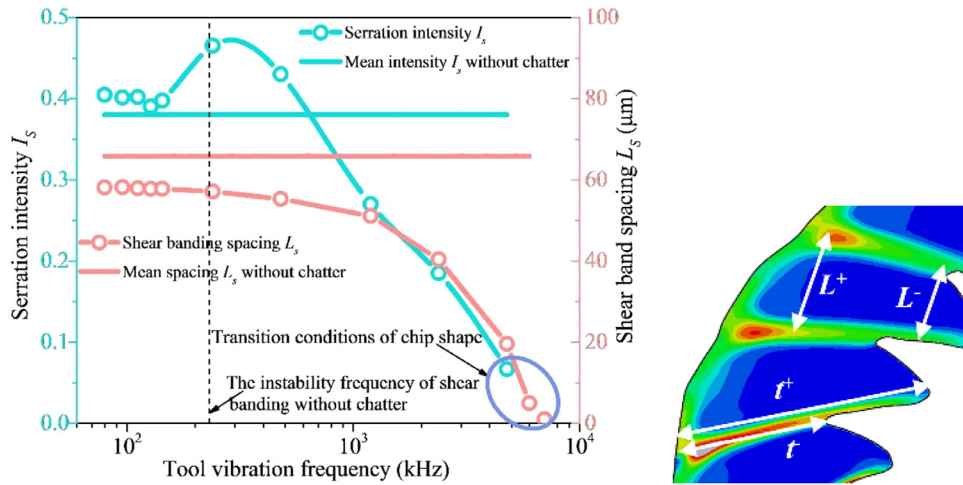


Fig. 7. The dependence of the mean shear band spacing and the segmentation intensity on the tool FV frequency as the cutting speed $V=20$ m/s. In the inset, the definitions of the shear banding spaces and the maximum and minimum chip thicknesses are shown.

frequency in vibration assisted machining is out of reach, the formation of shear bands should be avoided to assure that vibration takes positive effects.

The morphology of serrated chip in the FV cutting process can be represented by two geometrical parameters: the mean shear band spacing L_s and the segmentation intensity I_s [56]. They are defined as

$$L_s = \frac{L^+ + L^-}{2}, I_s = \frac{t^+ - t^-}{t^+} \quad (3)$$

where L^+ and L^- are two shear band spacing in different positions, and the maximum and minimum chip thicknesses, t^+ and t^- are introduced (see the inset of Fig. 7).

In terms of (3), the dependence of the serration intensity and the shear band spacing on FV frequency are plotted in Fig. 7. When FV frequency is much less than the instability frequency of shear bands 240 kHz, the segmentation intensity is nearly constant. When resonance occurs, i.e., the FV frequency equals 240 kHz, the segmentation intensity reaches the peak value, implying that the evolution of shear bands are promoted at the maximum degree. As the FV frequency exceeds 240 kHz, the segmentation intensity decreases rapidly, which represents evident transition tendency of the chip shape from serrated to continuous. The segmentation intensity approaching zero indicates complete transition into the continuous chip. In the low-frequency cutting process, the values of the segmentation intensity are always greater than the mean segmentation intensity without vibration, implying that the low-frequency FV promotes the evolution of shear bands. Moreover, the low-frequency FV has no obvious influence on the shear band spacing. The mean spacing in the FV cutting process, approximately a constant $58 \mu\text{m}$, is less than the mean spacing without vibration. As the tool FV frequency increases, the shear band spacing decreases monotonously until it approaches zero at the FV frequency of 7000 kHz, which means that serrated chip has turned into continuous chip completely due to the strong suppression of vibration on instability of shear banding.

Fig. 8 shows the simulation results of the cutting forces as the cutting speed $V=20$ m/s. It is well known that the oscillation frequency of cutting force is identical with the instability frequency of shear bands [54] (Fig. 8a). When the tool FV frequency is 120 kHz, the oscillation frequency of cutting force increase evidently but the amplitude decreases (Fig. 8b). At the resonance frequency 240 kHz, at which the oscillation of cutting force in amplitude reaches the greatest degree, meaning that the strongest impacting of FV on the cutting force presents (Fig. 8c). When the tool vibration frequency is 480 kHz, the high frequency oscillation of cutting force starts to appear over the low-frequency oscillation component (Fig. 8d), which shows that the plastic flow behavior of ma-

terial inside the shear bands starts to change in the sense of microscale. As the tool frequency is about 6000 kHz, the low-frequency oscillation of cutting force begins to disappear (Fig. 8e). When the tool frequency equals 7000 kHz, it disappears completely (Fig. 8f). At this moment, the serrated chip fully changes into the continuous chip.

Fig. 9 shows the Fourier transform results of cutting forces. The results in Fig. 9a demonstrates that the periodic shear banding instability has the ability to generate the oscillatory cutting force with high amplitude and low frequency. When the FV frequency is less than 6000 kHz (Fig. 9b and d), two high-amplitude integrant appear in the frequency domain, which correspond to the tool vibration and the periodic shear banding instability. Particularly, resonance leads to the greater amplitude at $f_T=240$ kHz (Fig. 9c). In this case, the oscillation force component from the periodic shear banding instability has the ability to produce the larger amplitude vibration in cutting force due to the storage of vibrational energy, and cause the damage on machining surface integrity and tool life. As the tool vibration frequency equals 6000 kHz, the critical value when the chip shape starts to transform from serrated to continuous again, the high-amplitude integrant of cutting forces distributes in both low- and high-frequency domains. The oscillation of cutting force is govern by the tool FV frequency and the multiple shear banding frequency. As the frequency exceeds 7000 kHz, only a high-amplitude integrant caused by tool vibration presents in high frequency domain, whereas the high-amplitude integrant in low frequency vanishes due to the formation of continuous chip.

FV with different frequencies can produce evident influence on the mean cutting forces. The curve in Fig. 10 shows the evolution the mean cutting force in FV with different frequencies based on the simulation results in Fig. 8. The mean cutting force is about 189.5 N/mm without vibration. For FV, the curve rises gradually in the low-frequency vibration domain and, after reaching the first peak value, decreases sharply to the minimum at the resonance frequency. In the high-frequency domain, it grows rapidly to the second peak value and then decreases gradually and finally shows a tendency towards the mean cutting force without vibration. It is worth noting that the resonance condition results in the minimum value of the mean cutting force, which doesn't mean that we can obtain the satisfactory surface integrity since the amplitude oscillation of cutting force reaches the maximum intensity at the same time. However, the evolution of the cutting force at the high-frequency vibration shows a good tendency, that is, the amplitude of the cutting force decreases linearly as the tool vibration frequency increases until the continuous chip develops. In the continuous chip formation, the tool FV makes the average cutting force decrease. However, in the high-speed cutting process, the periodic shear banding instability lead the average

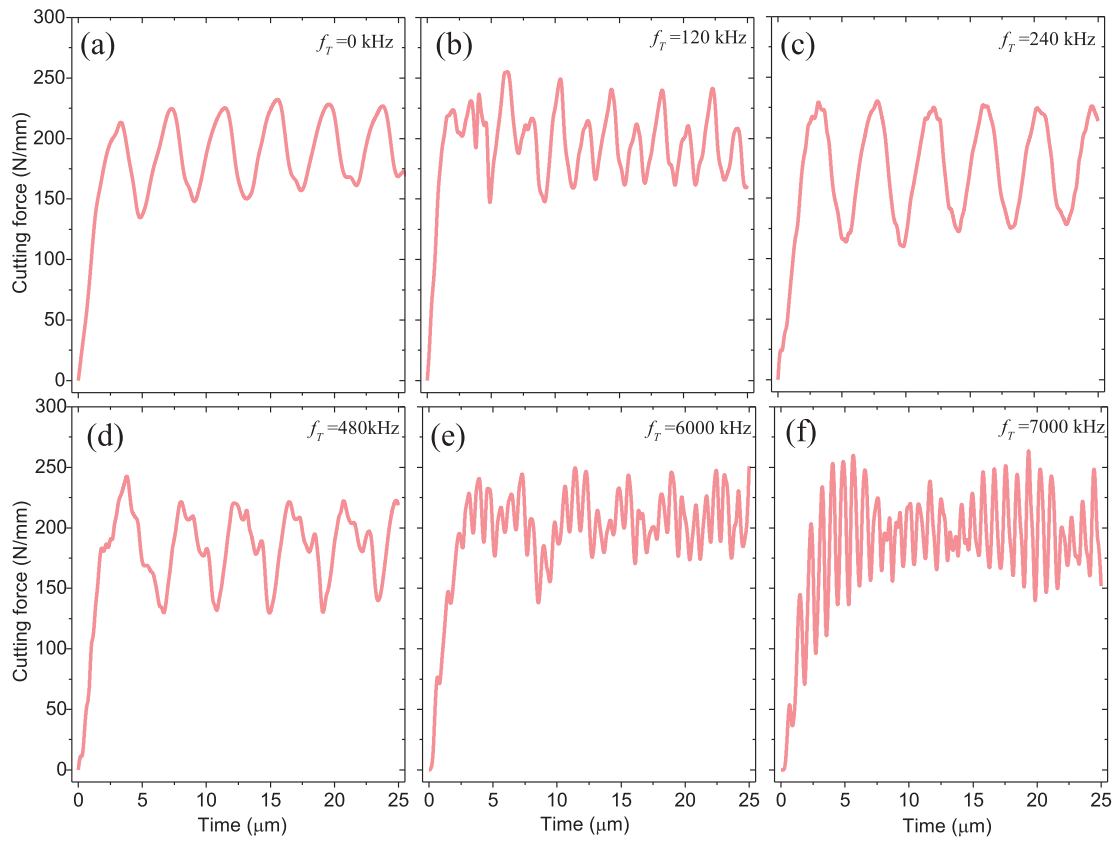


Fig. 8. The effects of tool FV frequencies on the cutting forces as $V = 20$ m/s.

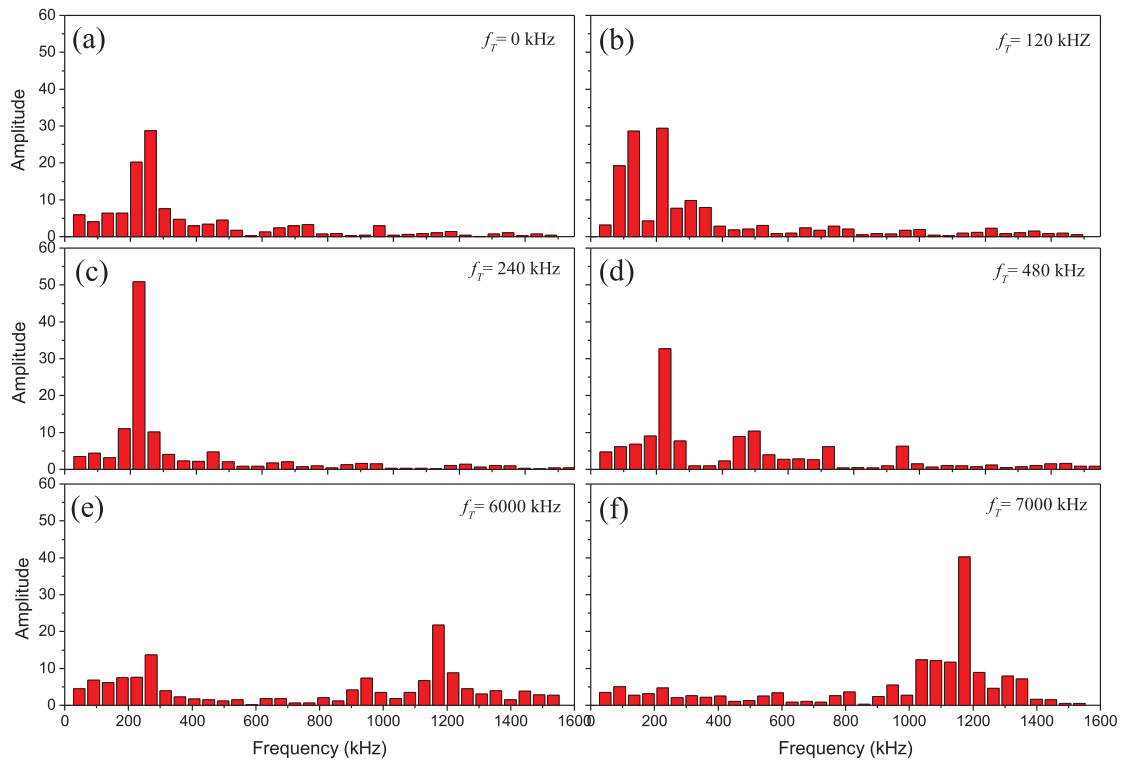


Fig. 9. The spectral analysis results of the cutting forces under the cutting speed $V = 20$ m/s.

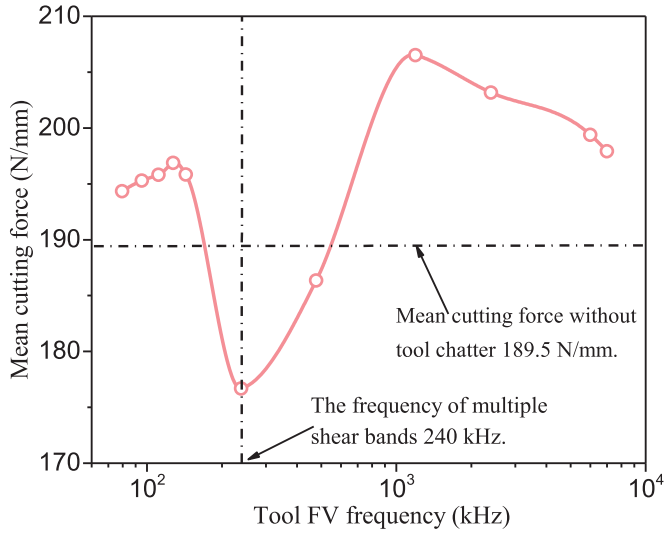


Fig. 10. The dependence of the mean cutting forces on the frequency of cutting tool as $V = 20$ m/s.

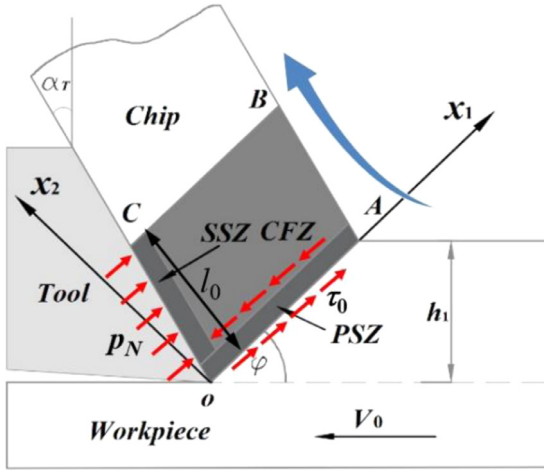


Fig. 11. The orthogonal cutting model used for the analysis of the chip flow stability.

cutting force to increase obviously. Only in the finite frequency domain with resonance frequency can the average cutting force decreases.

3.3. Analysis of chip flow stability

3.3.1. Instability criterion

Usually, the serrated chip in high-speed cutting process is attributed to the periodic shear banding formation as the thermo-plastic instability phenomenon. In the FV cutting process, the tool vibration changes the distributions of the shear stress in PSZ and the pressure on the tool-chip interface, which results in a more complex thermo-plastic instability behavior of cutting material. In order to get a clear insight into the chip flow behavior in the FV cutting process, a linear stability analysis on the plastic flow of chip material is performed in terms of the orthogonal cutting model [61,62]. In this model, the influence of the pressure on the tool-chip face on the cutting force is considered similar to Burns and Davies [63] (Fig. 11).

The basic equations governing the thermo-mechanical deformation of PSZ material include: the momentum conservation equation:

$$\rho \frac{\partial^2 \gamma}{\partial t^2} = \frac{\partial^2 \tau}{\partial y^2} \quad (4)$$

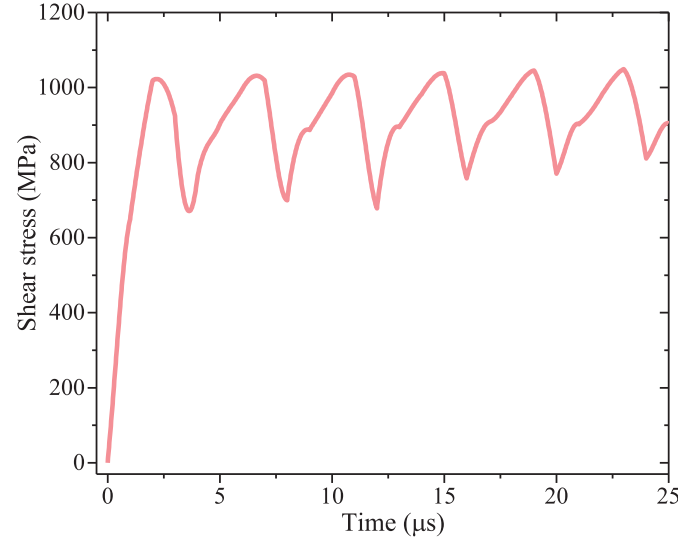


Fig. 12. The variation of shear stress on the shear plane with time as the cutting speed $V = 20$ m/s and the FV frequency $f_T = 240$ kHz.

the energy conservation equation:

$$\rho c \frac{\partial T}{\partial t} = \lambda \frac{\partial^2 T}{\partial y^2} + \beta \tau \dot{\gamma} \quad (5)$$

where ρ , c and λ are the density, specific heat, thermal conductivity of work-material. β is the Taylor-Quinney coefficient.

Fig. 12 shows that the evolution of shear stress at the resonance frequency in the FV simulation. To consider the influence of tool vibration, the shear stress component is assumed known based on Fig. 12 and has the form of sinusoidal function:

$$\tau_0 = \tau' + \tau'' \sin(2\pi f_T t + \phi) \quad (6)$$

where t is time, τ' is the shear stress component without vibration, τ'' , f_T and ϕ is the amplitude, frequency and the phase angle of the shear stress component in vibration. Similar to Burns and Davies [63], the shear stress τ , pressure p_N and the cutting speed V_0 have the relationship as follows.

$$\frac{\partial \tau_0}{\partial t} = \frac{l_0 \sin \phi}{h_1} \frac{dp_N}{dt} = \frac{El_0 \sin^2 \phi}{h_1^2} (V_0 \cos \phi - \dot{\gamma} h_1) \quad (7)$$

where E is the elastic modulus, l_0 the contact length between tool and chip on the rake face and h_1 the cut depth.

When carrying out the analysis of chip flow stability, the small perturbation method is used to governing Eqs. (4), (5) and the J-C law (1) to seek an inhomogeneous deformation solution with respect to the homogeneous solution. Assuming that

$$\begin{Bmatrix} \tau \\ \gamma \\ T \end{Bmatrix} = \begin{Bmatrix} \tau_0 \\ \gamma_0 \\ T_0 \end{Bmatrix} + \begin{Bmatrix} \tau^* \\ \gamma^* \\ T^* \end{Bmatrix} \exp(\omega t +iky), \quad \begin{Bmatrix} \tau_0 \\ \gamma_0 \\ T_0 \end{Bmatrix} \ll \begin{Bmatrix} \tau^* \\ \gamma^* \\ T^* \end{Bmatrix} \quad (8)$$

where τ_0 , γ_0 and T_0 is a group of homogeneous solution of the governing equation system. τ^* , γ^* and T^* are small constants characterizing the initial magnitude of perturbation, ω is the initial perturbation growth rate and k is the wave number.

Inserting Eq. (8) into Eqs. (1), (4) and (5), only considering the first order terms of the perturbations, we obtain the characteristic equation about the perturbation growth rate ω as follows:

$$\hat{\omega}^3 + (1+A)\hat{k}^2 \hat{\omega}^2 + [(A\hat{k}^2 + 1 - B)\hat{k}^2 + C]\hat{\omega} + \hat{k}^4 + D\hat{k}^2 = 0 \quad (9)$$

In (9), the following dimensionless variables are used:

$$\hat{\omega} = \frac{\lambda \omega}{c Q_0}, \hat{k}^2 = \frac{\lambda^2 k^2}{\rho c^2 Q_0}, A = \frac{c R_0}{\lambda}, B = \frac{\beta P_0 \tau}{\rho c Q_0}, C = \frac{\lambda^2 \gamma_0 \beta P_0}{\rho c^3 Q_0^2}, D = \frac{\beta P_0 \lambda E l_0 \sin^2 \phi (\gamma_0 \delta_1 - V_0 \cos \phi)}{\rho c^2 Q_0^2 h_1^2} \quad (10)$$

where Q_0 is the strain hardening factor of the material, R_0 is strain-rate hardening factor, and P_0 is thermal softening factor. The stability of chip flow depends on the value of dimensionless growth rate. If it goes negative, the chip flow is stable; otherwise, the plastic flow instability is possible. The negative term in the first power of the growth rate in (9) ensure that the characteristic Eq. (9) has at least one positive real root. This means that the chip plastic flow may develop continuously until the plastic instability occurs at a special set of wave numbers. Therefore, based on the extreme condition $d\hat{\omega}/d\hat{k}_m^2 = 0$, the criterion for evaluating the plastic instability of chip flow in the vibration cutting process can be found as follows:

$$F_{Inst} = \frac{(I_0 + I_1 - I_2)\beta P_0}{\rho c Q_0} > 1 \quad (11)$$

where

$$I_0 = \tau_0, I_1 = \tau' \sin(2\pi f_T t + \phi), I_2 = 2\sqrt{\frac{\rho c R_0 I_0 \sin \phi \dot{p}_N}{h_1 \beta P_0}},$$

$$\dot{p}_N = \frac{2\pi f_T \tau' h_1}{I_0 \sin \phi} \cos(2\pi f_T t + \phi) \quad (12)$$

In the instability criterion (11), the nominator of the instability function F_{Inst} represents the thermal softening effect of chip material and the denominator denotes the strain hardening effect of material. Thus, if the value of F_{Inst} is greater than one, it means that the plastic flow is possibly unstable; otherwise, the plastic flow is stable. The first term in the nominator denotes the thermal softening effect produced by the shear stress τ_0 in the cutting process without the tool vibration. The second and third terms represent respectively the effects of the shear stress oscillation in the PSZ and the pressure oscillation at the tool-chip interface on the thermal softening in the vibration cutting process. In the accordance with the modeling result in Fig. 3c and Fig. 8a, the expression of the shear stress τ_0 can be found through the curve fit of sine function as

$$\tau_0 = \tau'_{SB} + \tau''_{SB} \sin(2\pi f_{SB} t + \phi_{SB}) \quad (13)$$

where $f_{SB} = 240$ kHz and $\phi_{SB} = -\pi$ are the instability frequency and initial phase angle of the cyclic shear bands. $\tau'_{SB} = 888$ MPa and $\tau''_{SB} = 323$ MPa are the mean shear stress and the amplitude of the shear stress oscillation, respectively.

3.3.2. Results and discussion

The expression of the instability function F_{Inst} indicates that FV can induce evident change of the thermal softening effect of material, but doesn't affect the strain hardening effect. Since the shear-localized deformation of material within PSZ is closely related to the thermal-softening effect, we can say that, the influence of FV on the evolution of the shear bands is by changing the thermal softening effect of material rather than changing the strain hardening effect. To clearly reveal the influence of FV on the shear banding instability, we can consider it in two steps.

Firstly, consider the influence of the shear stress oscillation on thermal softening of material within shear bands. The parameters in the shear stress oscillation factor I_1 in (12) are taken as $\tau' = \tau'_{SB}$ and $\phi = \phi_{SB}$ in terms of the simulation results in Fig. 8. In the FV cutting process with the cutting speed $V = 20$ m/s, the instability frequency of shear bands is $f_{SB} = 240$ kHz. For the different FV frequencies, the shear stress oscillation aggravates the thermal softening effect of material, however, in the average sense, doesn't change the total thermal softening effect as shown in Fig. 13. The low-frequency oscillation of shear stress with $f_T < f_{SB}$ has a tendency to reduce the instability frequency of shear bands (Fig. 13b). In the resonance case of $f_T = f_{SB}$, the oscillation of shear stress generates the strongest thermal softening effect of material (Fig. 13c). The high-frequency oscillation of shear stress with $f_T > f_{SB}$ doesn't affect the frequency of periodic shear banding instability, but results in the micro-mechanism variation of plastic flow of material. That is, the shear banding evolution is accompanied with the high frequency oscillation of material points (Fig. 13d-f). The energy required for this material

softening mechanism is provided by the work done by the oscillating shear stress. The oscillation of shear stress induces the increase on the oscillatory amplitude softening factor even though it doesn't change the average degree of thermal softening of materials. In this sense, it is beneficial to the evolution of shear bands.

Secondly, consider the combined effects of the shear stress and the pressure on the thermal softening effect of material within shear bands. In present analysis, same oscillation frequencies of the shear stress and the pressure are used and the results are shown in Fig. 14. In the cases of the low-frequency oscillation $f_T < f_{SB}$ and the resonance $f_T = f_{SB}$, the combined effect still aggravates the softening effect of material relative to the case without oscillation (Fig. 14a), implying that it promotes the evolution of shear bands (Fig. 14b and c). However, comparing with the cases without pressure in Fig. 13b and c, the softening effect is evidently weakened due to the existence of pressure oscillation. An obvious feature is that the average degree of material softening is significantly reduced and the other is the oscillatory amplitude of softening factor is also appropriately decreased. With the further increase of oscillation frequency as $f_T > f_{SB}$, the combined effect completely changes the materials softening mechanism. Not only the oscillation amplitude of the softening factor evidently decreases, but also the thermal softening degree has become negative in the average sense. Particularly, the oscillation of periodic shear banding instability has disappeared completely (Fig. 14d-f). This implies that the high-frequency pressure oscillation has dominated the thermal softening mechanism of chip material, suppressed the evolution of shear bands and made the continuous chip develop fully.

Consistent with simulation results, FV exhibits different influence on the evolution of shear bands. In the high-speed cutting process with tool FV, the shear stress oscillation promotes the development of the softening effect of material within shear bands. In the process, the work done by the shearing force is transformed into the shear localized deformation energy of PSZ material. Therefore, the shear stress oscillation makes the occurrence of periodic shear banding instability of chip material easier. Conversely, the pressure oscillation always weakens the material softening effect. In the low-frequency FV cutting, the promoting effect of shear stress oscillation for the evolution of shear bands overcomes the depression effect of pressure oscillation, so shear banding evolution is promoted overall. However, in the high-frequency FV cutting, pressure oscillation consumes most of the energy required by the shear banding formation and evolution, which forcefully restrains the evolution of the shear bands in the serrated chip, and results in the transition of serrated chip into the continuous chips.

4. Self-excited vibration cutting process

4.1. Simulation of the self-excited vibration cutting process

4.1.1. The double-tool model

The nonlinear dynamics in the SEV cutting process is related to the cutting conditions, tool geometry and the machined wavy surface. In order to simulate the SEV cutting process, a double-tool cutting model is designed as shown in Fig. 15. In this model, the tools are described by the Lagrangian elements with material mesh, and the plastic flow of the workpiece material is described by the Eulerian elements with spatial mesh. The size of Eulerian mesh is set as $3 \mu\text{m}$ and the inclination angle is 45° relative to the horizontal direction. The tool-1 carries out the FV cutting with a prescribed vibration frequency in y-axial direction, which represents the structural dynamics of machine tool system and can generate the wavy machined surface for the following SEV cutting. When the parameters of the tool-1 FV motion are prescribed, corresponding SEV cutting process of tool-2 are also determined. In high-speed cutting process, the tool-2 SEV stems from two sources: the wavy cut thickness and the formation of periodic shear bands. The top wavy surface produced by the tool-1 FV cutting is described as

$$y_1 = y_{10} + A_{w1} \sin(\omega_{w1} t + \theta_{w1}) \quad (14)$$

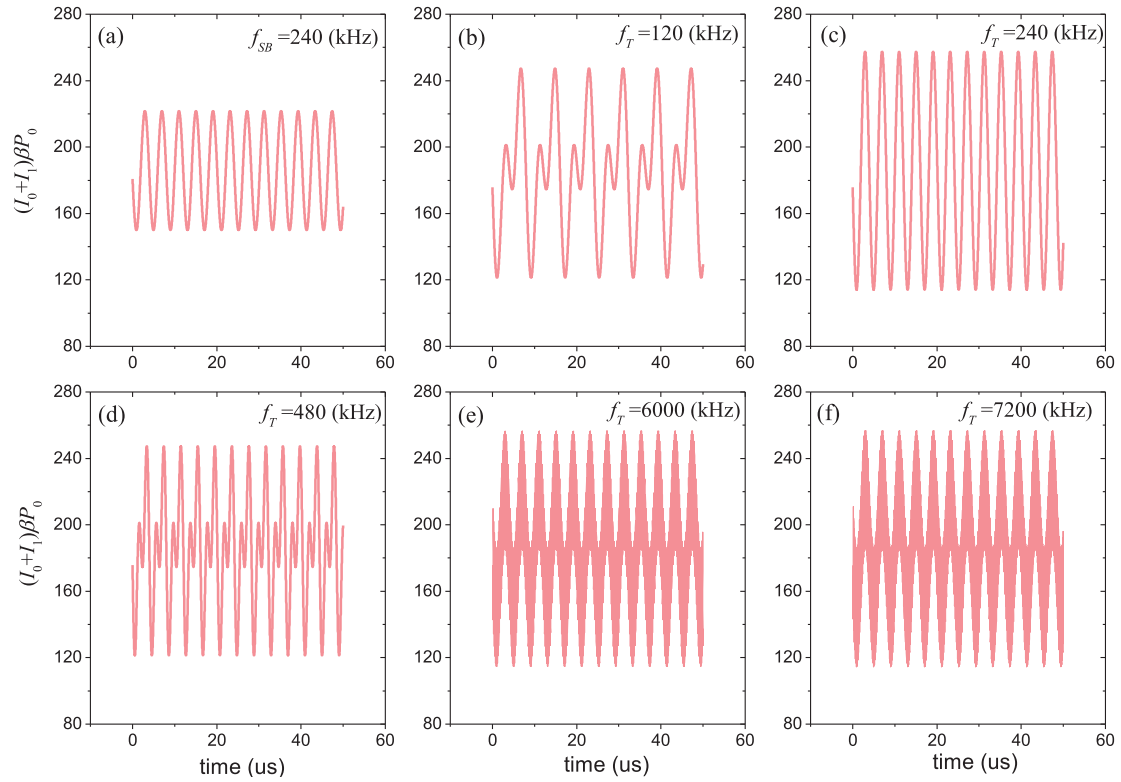


Fig. 13. The thermal softening effect of material within shear bands caused by the shear stress oscillation with different frequencies.

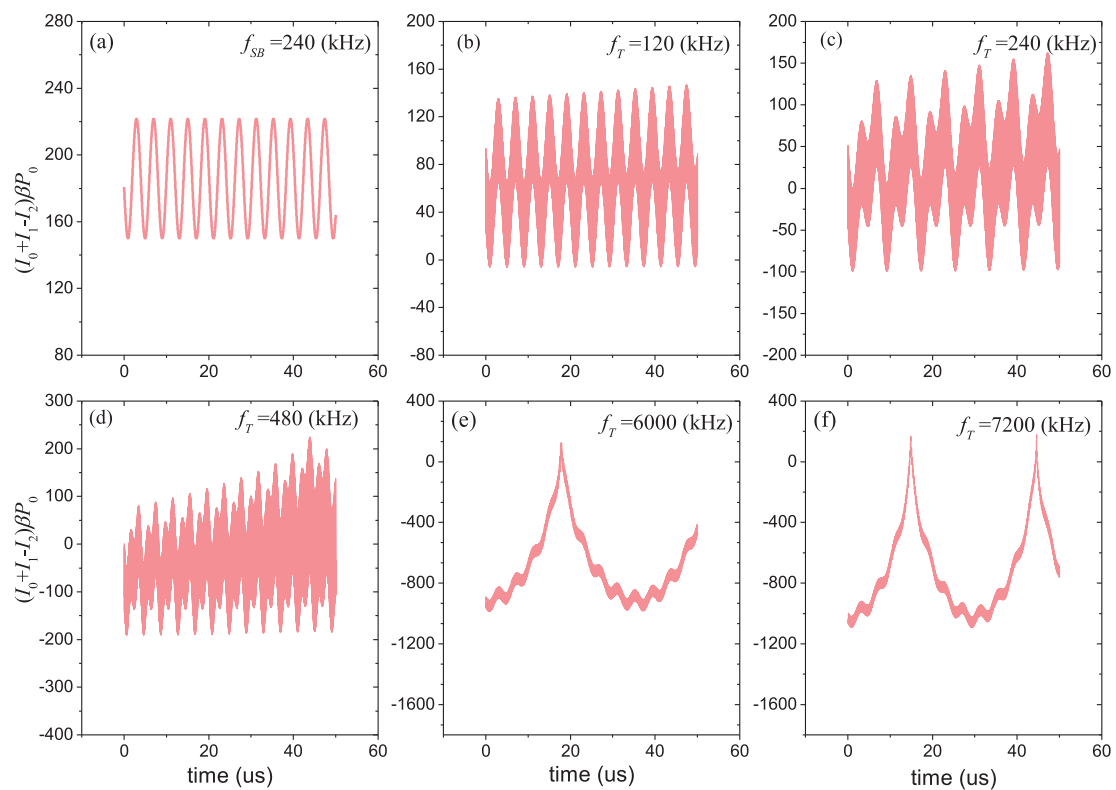


Fig. 14. The thermal softening effect of material within shear bands caused by the shear stress oscillation and the pressure oscillation with different frequencies.

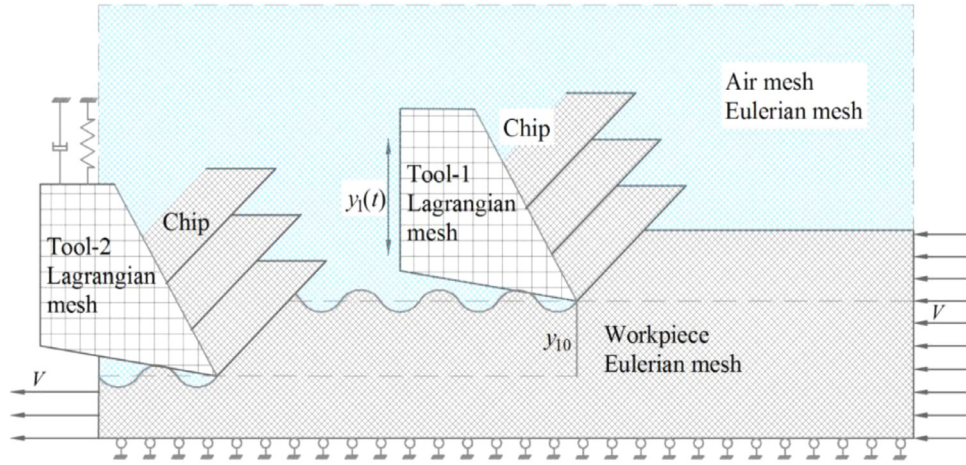


Fig. 15. The double-tool FE model for the simulation of the tool SEV cutting process.

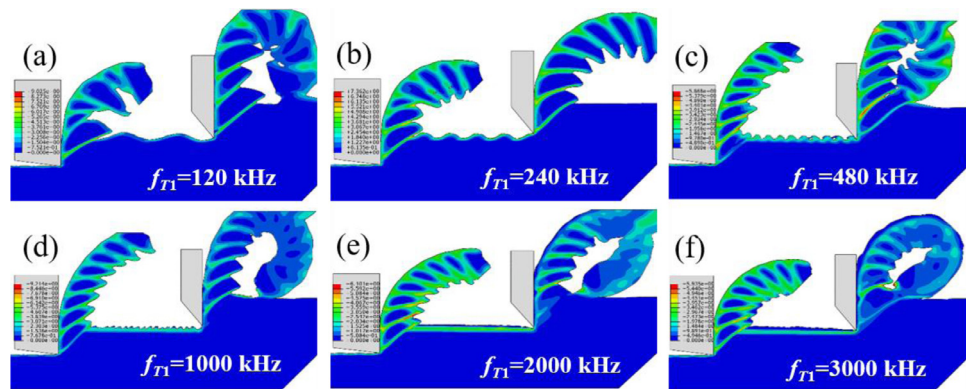


Fig. 16. The contours of equivalent plastic strain under different vibration frequency of tool-1 ($V = 20$ m/s).

where y_1 denotes the vertical oscillation displacement of the tool-1 at time t , $\omega_{w1} = 2\pi f_{T1}$ the angular velocity of the tool-1 vibration, f_{T1} the vibration frequency, θ_{w1} the initial phase angle and A_{w1} the vibration amplitude. The average cut depth is $y_{10} = 100 \mu\text{m}$, the cutting distance is $500 \mu\text{m}$ and the cutting speed is $V = 20$ m/s. Under these cutting conditions, the plastic flow of Ti6Al4V alloy chip is unstable and leads to the formation of serrated chip.

4.1.2. The simulation results and discussion

The resulting equivalent plastic strains of workpiece show that the chip morphology in the SEV cutting depends on the FV frequency of tool-1 (Fig. 16). The wavy machined surface produced in the tool-1 FV cutting produces the wavy cut thickness for the following SEV cutting process. For the FV frequency $f_{T1} = 120$ kHz, the generated wavelength of wavy machined surface is larger than the shear band spacing, so that more than one shear bands can develop in one wavy period in the SEV cutting. Specifically, the longer shear bands form in the large chip thickness and the shorter shear bands form in small chip thickness. Since the cutting work done by the tool-2 to workpiece is constant under unchanged cutting speed condition, only one longer shear band forms but more than one shorter shear bands might appear (Fig. 16a and b). Oscillation frequency of wavy machined surface rises with increasing FV frequency of tool-1, which makes the chip thickness in the SEV cutting process tend rapidly to be homogeneous. As a result, the multiple shear banding instability tends to be steady and the serrated chip has uniform thickness and serrated size as shown in Fig. 16c to f. Compared with the result without vibration in Fig. 3c, SEV can decrease serration intensity of serrated chip to different degrees. Smoother upper surface generated by higher FV frequency corresponds to the maximum suppression of serrated chip. The simulation results also demonstrate that the frequency

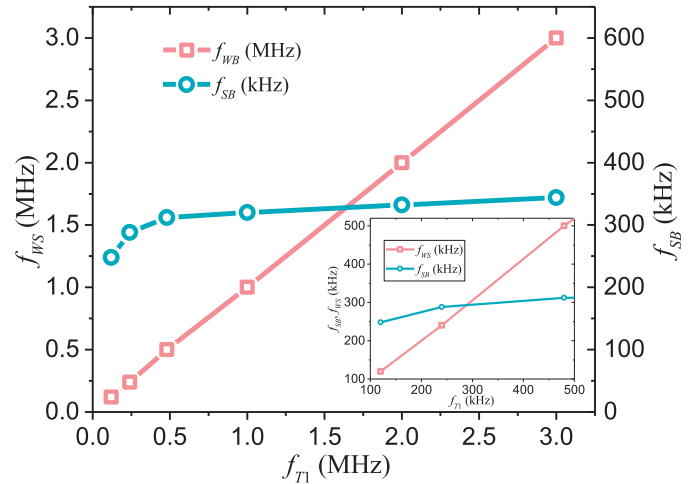


Fig. 17. The relationships among the frequency of the tool-1 FV, the wavy surface oscillation and the frequency of shear banding instability of the chip produced in the SEV cutting process.

of the wavy machined surface f_{WB} is linearly proportional to the tool-1 FV frequency f_{T1} . The multiple shear banding instability f_{SB} is more sensitive to the low FV frequency than the high FV frequency as shown in Fig. 17.

Fig. 18 illustrated the modeling results of the cutting forces and ploughing forces of tool-2 SEV with different tool-1 FV frequencies. For comparison, the modeling result of conventional cutting force is also drawn in this figure. In the low-frequency cutting process, the tool-2 SEV

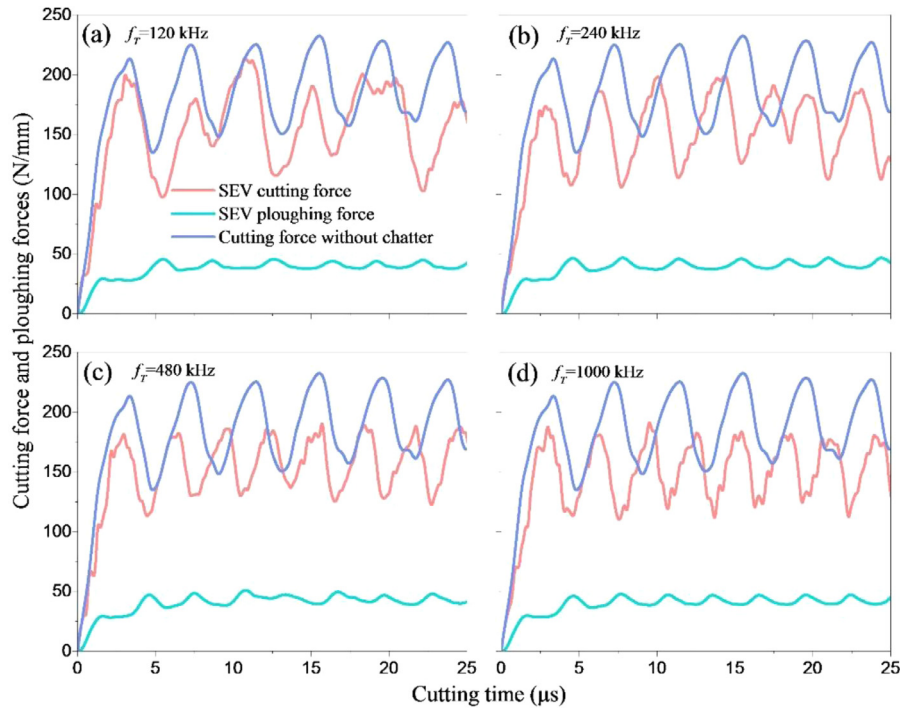


Fig. 18. The cutting forces and ploughing forces of tool-2 SEV vary with the cutting time ($V=20$ m/s).

cutting process gets into a non-uniform oscillatory state after the onset of cutting. The average SEV cutting forces decrease obviously with increasing tool-1 FV frequency. The low-frequency FV induces slight variation of shear banding instability frequency (Fig. 18a). When the FV frequency is above 240 kHz, the frequency of shear banding instability evidently rises with increasing FV frequency (Fig. 18b-d). This is because that the variation of wavy chip thickness changes the oscillation period of cutting forces. In the cutting process with constant speed, the variation chip thickness generated by different frequency FV strongly affects the material softening and strain rate sensitivity of work-material, which change the shear banding instability behavior of chip-material and result in the oscillation of cutting force with varying amplitude and period. For high FV frequency, the fluctuation of the wavy chip thickness is significantly reduced, which greatly weakens the influence of the variation of wavy chip thickness on the cutting force, and thus, the oscillation frequency of cutting force approaches to the instability frequency of shear bands and the oscillation amplitude of cutting force tends to uniform again.

Fig. 19 presents the displacement evolution of tool-2 with time. In the SEV cutting process, the wavy cutting thickness is determined by the relative displacement between tool-1 and tool-2. If the relative phase difference between the two machining wavy surfaces is zero, the variation of wavy chip thickness is also zero. If the relative phase difference is π , the variation of the chip thickness is maximum. On the other hand, the variation of cutting thickness in the SEV cutting determines the cutting force oscillation. Comparing with the simulation results of cutting force in Fig. 18, we can see that the SEV displacement has same relative phase angle as that of the ploughing force, but has opposite phase angle of as that of the cutting force. Consequently, the wavy cutting thickness affects the cutting force, and the oscillation of wavy surface affects the ploughing force. In the high-speed cutting process, the influences of the changing cutting thickness and wavy surface become non-evident and the multiple shear banding instability controls the cutting force in the SEV cutting process. The oscillation frequency of the tool-2 displacement approaches to the shear banding instability frequency. Compared with conventional cutting without vibrations, SEV can decrease cutting force stably with higher FV frequency. Thus, it is SEV with smooth cutting thickness, instead of FV with too high frequency, could be an effective strategy to suppress the evolution of shear bands, im-

prove machined quality and alleviate tool wear in the high-speed cutting process.

4.2. Theoretical analysis of tool-2 self-excited vibration process

In this subsection, we carry out the stability analysis of tool-2 in SEV cutting process. The analytical model is shown in Fig. 20. The top wavy surface of workpiece is produced in the tool-1 FV cutting. In SEV cutting process, tool-2 is assumed as a spring-mass-damper system with single degree of freedom. The motion of tool-2 is limited in the y-axis direction. The average cut depth with the wavy surface, the rake angle and the shear angle are denoted by y_0 , α and φ , respectively. We further assume that the tool system has the equivalent mass m_0 , constant equivalent stiffness k_0 and damping coefficient μ_0 . The forces of the tool-2 acting on the chip and workpiece include the cutting force F_y in the horizontal direction and the ploughing force f_y in the vertical direction. A stationary coordinate system xOy is attached to the symmetry plane of the tool-workpiece machine system, and $y_2(t)$ represents the transient vertical position of the tool-2 tip at time t . If the assumption of small amplitude vibration for the tool-2 system SEV is used, the equation of motion can be written as:

$$m_0 \ddot{y}_2 + \mu_0 \dot{y}_2 + k_0 y_2 = (-F_y) + (-f_y) \quad (15)$$

During the SEV cutting process, the tool-2 vibration stems from the perturbations caused by the varying cut depth due to the top wavy surface and the formation of multiple shear bands in the serrated chip. The cutting force F_y is represented as [64]:

$$F_y = -\frac{(y_1 - y_2)w\tau \sin(\beta - \alpha)}{\sin \varphi \cos(\varphi + \beta - \alpha)} \quad (16)$$

where τ is the shear stress on the shear plane, $\beta = \tan^{-1}(\mu)$ is the friction angle, μ is the friction coefficient of the tool-chip interface, the rake angle α is set to zero and w is the cut width. In terms of the small vibration assumption, only the effect of the top wavy surface on the cut depth is considered in the present analysis and the influence of the variation of rake angle is ignored. Thus, the undulation of the top wavy surface with the average cut depth y_0 can be written in the form (Fig. 20):

$$y_1 = y_0 + A_{w0} \sin(\omega_w t + \theta_w) \quad (17)$$

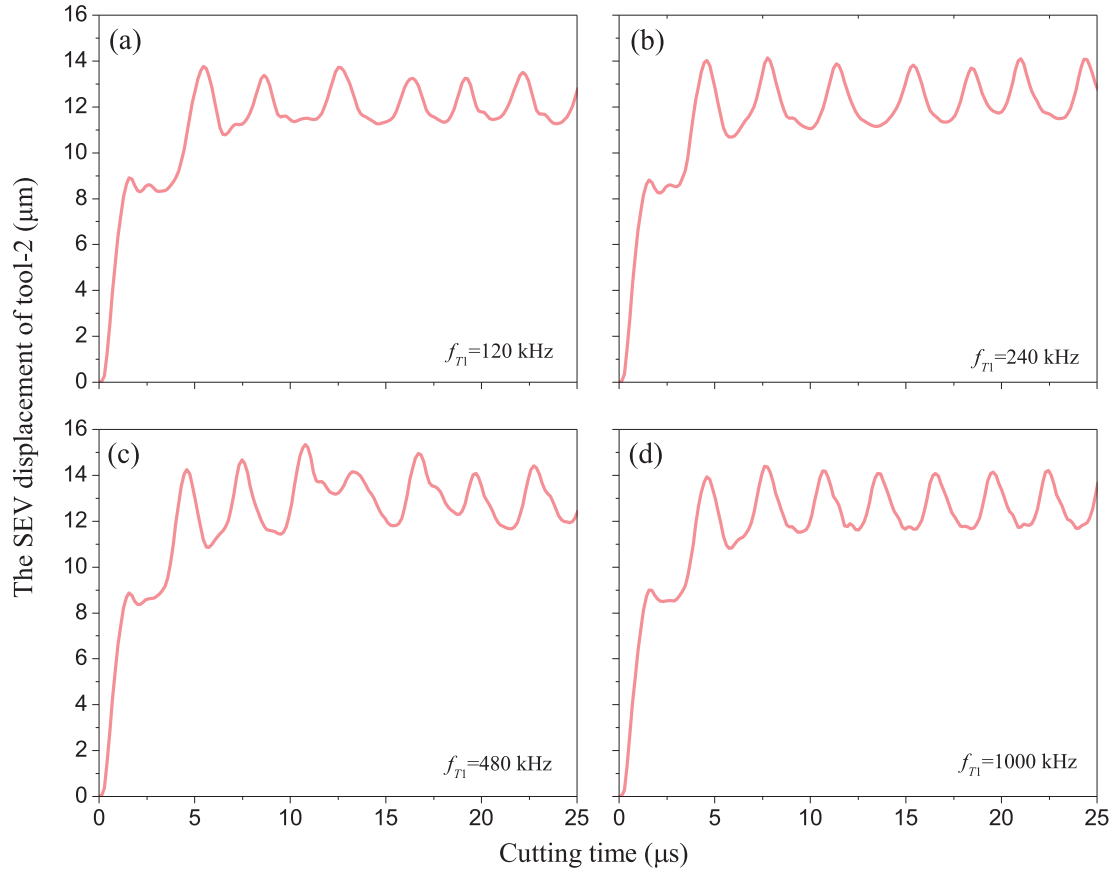


Fig. 19. The displacements of tool tip in the tool-2 SEV process vary with the cutting time ($V = 20$ m/s).

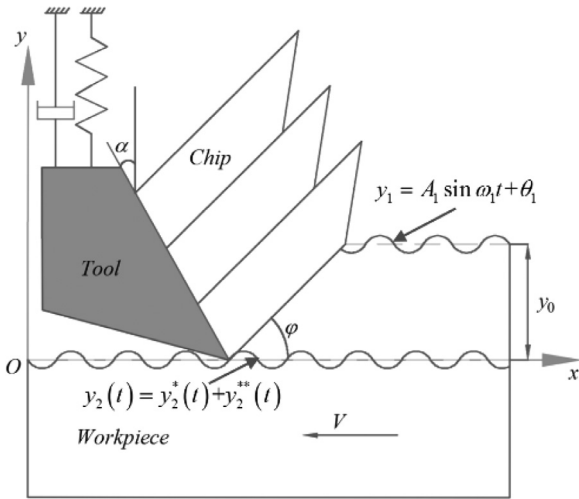


Fig. 20. The analytical model of the cutting process with tool-2 SEV motion.

where A_{w0} denotes the oscillation amplitude of wavy surface, ω_w the angular velocity of wavy surface oscillation, and θ_w the initial phase angle. The Eq. (17) is identical to that of the tool-1 vibration in (14). In the high-speed cutting process, the shear stress in PSZ varies with the periodic formation of shear bands. Suppose that the shear stress is a periodic function of time t :

$$\tau = \tau_0 + A_{s0} \sin(\omega_s t + \theta_s) \quad (18)$$

where τ_0 is the mean shear stress, A_{s0} the oscillation amplitude of shear stress, ω_s the angular velocity of shear banding instability and θ_s the initial phase angle.

According to Wu and Liu [64] and Kudinov et al. [65], the role of the ploughing force f_y is evident in the SEV cutting process and it is assumed to be linearly dependent on the time rate of tool-2 displacement:

$$f_y = \frac{\mu_c w}{V} \dot{y}_2 \quad (19)$$

where μ_c is the cutting damping coefficient. By inseting Eqs. (16) to (19) into Eq. (15) and only remain the linear terms, the equation of motion governing the tool-2 SEV process can be written as:

$$\ddot{y}_2 + 2\Xi\Omega_n \dot{y}_2 + \Omega_n^2 y_2 = C_0 [1 + A_w \sin(\omega_w t + \theta_w)] [1 + A_s \sin(\omega_s t + \theta_s)] \quad (20)$$

where the equivalent relative damping coefficient Ξ and the equivalent angular velocity Ω_n of the tool-2 system are introduced and can be defined as follows:

$$2\Xi\Omega_n = 2\xi\omega_n - \frac{\mu_c w}{m_0 V}, \Omega_n^2 = \omega_n^2 - \frac{C_0}{y_0},$$

$$2\xi\omega_n = \frac{\mu_0}{m_0}, \omega_n^2 = \frac{k_0}{m_0}, C_0 = \frac{y_0 \tau_0 w \sin \beta}{m_0 \sin \varphi \cos(\varphi + \beta)}, A_w = \frac{A_{w0}}{y_0}, A_s = \frac{A_{s0}}{\tau_0} \quad (21)$$

In (21), ξ and ω_n are relative damping coefficient and the inherent angular velocity of the tool-2 SEV. In the derivation of the Eq. (20), the influence of the shear stress oscillation on the equivalent angular velocity Ω_n has been neglected. From Fig. 20, we can see that the equivalent relative damping coefficient Ξ is sensitivity to the cut width as the cutting speed is less than 10^3 m/s and its values are greater than one as the cutting speed is less than 60 m/s for the cut width 1 μ m.

To solve the Eq. (20), two cases are considered:

Case 1: When $\Xi^2 - 1 \geq 0$, the general homogeneous solution of the Eq. (20) is:

$$y_2^*(t) = C_1 e^{\omega^* t} + C_2 e^{\omega^- t} \quad (22a)$$

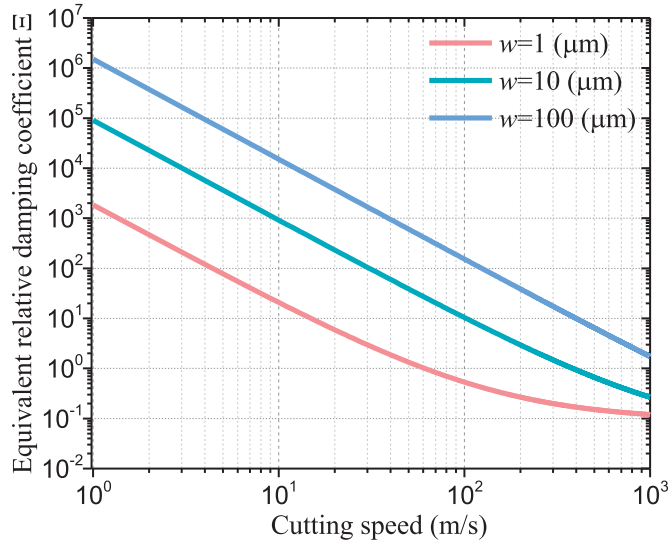


Fig. 21. The dependence of the equivalent relevant damping coefficient on the cutting speed at different cut width.

where

$$\omega^+ = -\Omega_n(\Xi + \sqrt{\Xi^2 - 1}), \omega^- = -\Omega_n(\Xi - \sqrt{\Xi^2 - 1}) \quad (22b)$$

Case 2: When $\Xi^2 - 1 < 0$, the general homogeneous solution is:

$$y_2^*(t) = e^{-\Xi\Omega_n t} (C_1 \cos \omega t + C_2 \sin \omega t) \quad (23a)$$

where

$$\omega = \Omega_n \sqrt{1 - \Xi^2} \quad (23b)$$

and C_1 and C_2 are the undetermined constants. The results in Fig. 21 show that the condition $\Xi^2 > 1$ is true as the cutting speed equals to 20 m/s. Thus, case 1 is meaningful and will be considered below. To solve for the complete solution of the Eq. (20), it is necessary to seek the particular solution of Eq. (20) $y_2^{**}(t)$. The completed solution of Eq. (6) is set with the form

$$y_2(t) = y_2^*(t) + y_2^{**}(t) \quad (24)$$

where $y_2^*(t)$ is given in (22) and $y_2^{**}(t)$ is found as:

$$y_2^{**}(t) = \frac{C_0}{\Omega_n^2} + \sum_{i=1}^2 \left[\Psi_i \sin(\omega_{\Pi_i} t + \Theta_{\Pi_i}) + (-1)^{i+1} \Psi_{i+2} \cos(\omega_{\Pi_{i+2}} t + \Theta_{\Pi_{i+2}}) \right] \quad (25)$$

The parameters in expression (25) are defined as:

$$\begin{aligned} \Psi_1 &= \frac{C_0 A_{\Pi_1}}{\Gamma_1}, \Psi_2 = \frac{C_0 A_{\Pi_2}}{\Gamma_2}, \Psi_3 = \frac{C_0 A_{\Pi_1} A_{\Pi_2}}{2\Gamma_3}, \Psi_4 = \frac{C_0 A_{\Pi_1} A_{\Pi_2}}{2\Gamma_4} \\ \Theta_{\Pi_i} &= \theta_{\Pi_i} - \theta_{\omega_{\Pi_i}}, \Theta_{\Pi_{i+2}} = \theta_{\Pi_{i+2}} - \theta_{\omega_{\Pi_{i+2}}} \\ \Gamma_i &= \sqrt{(\Omega_n^2 - \omega_{\Pi_i}^2)^2 + (2\Xi\Omega_n\omega_{\Pi_i})^2}, \theta_{\omega_{\Pi_i}} = \arctan \left[\frac{2\Xi\Omega_n\omega_{\Pi_i}}{\Omega_n^2 - \omega_{\Pi_i}^2} \right] \\ \omega_{\Pi_3} &= \omega_{\Pi_1} - \omega_{\Pi_2}, \omega_{\Pi_4} = \omega_{\Pi_1} + \omega_{\Pi_2}, \theta_{\Pi_3} = \theta_{\Pi_1} - \theta_{\Pi_2}, \theta_{\Pi_4} = \theta_{\Pi_1} + \theta_{\Pi_2} \end{aligned} \quad (26)$$

where Π_i ($i = 1, 2, \dots, 4$) stand for $w, s, w-s$ and $w+s$, respectively, and subscripts w and s denote respectively the wavy surface and the shear bands. $\Theta_{\Pi_i} = \theta_{\Pi_i} - \theta_{\omega_{\Pi_i}}$ is the equivalent phase difference. Using the boundary conditions $y_2(0) = \dot{y}_2(0) = 0$, the values of the constants C_1 and C_2 in

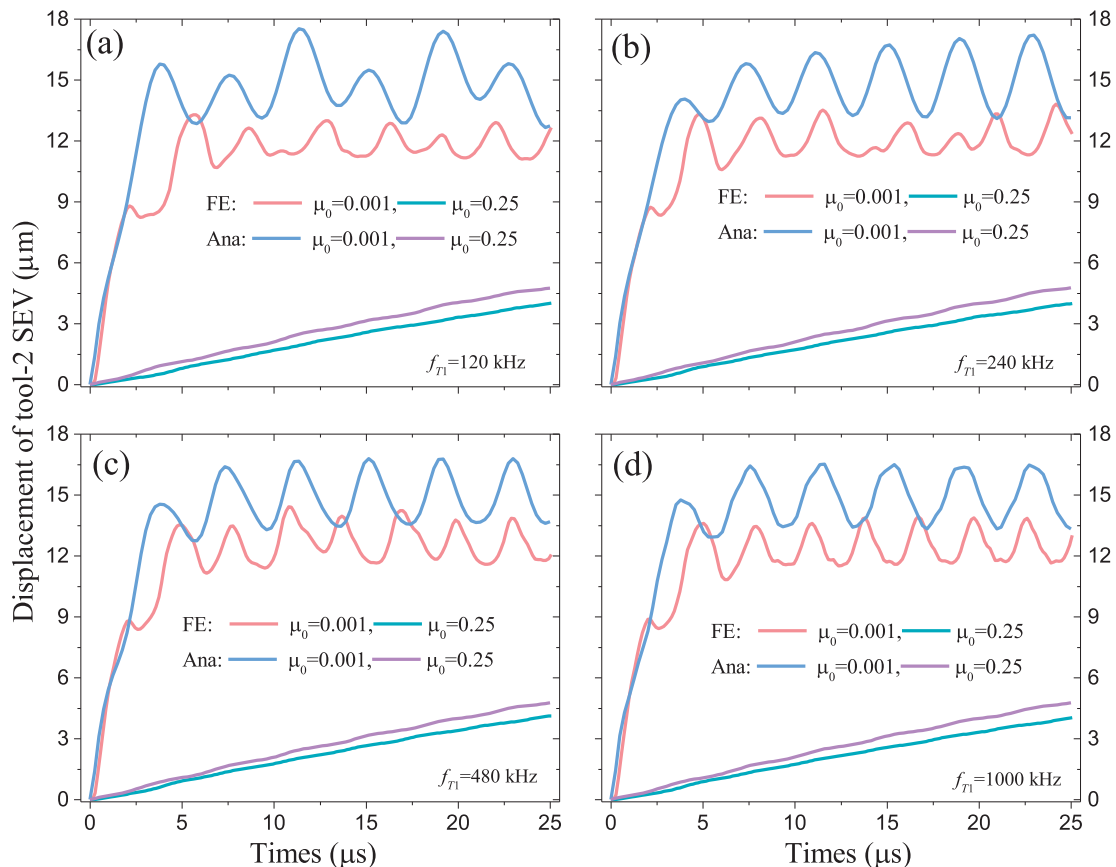


Fig. 22. The tool-2 SEV displacement-time curves at different relevant damping coefficients ($V = 20$ m/s).

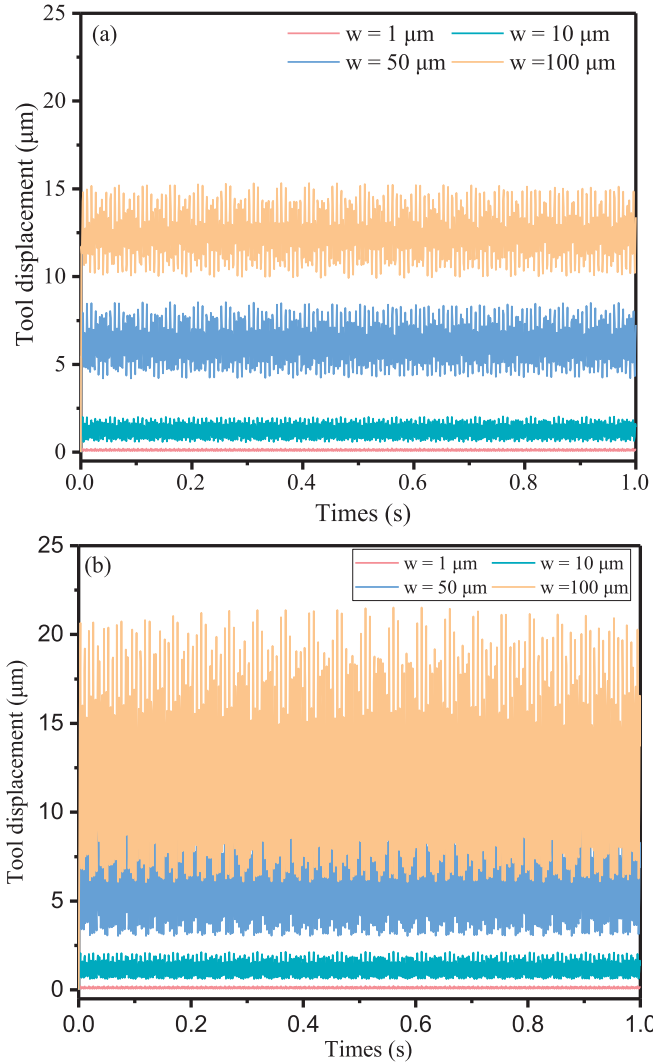


Fig. 23. The effect of the additional damping in cutting on the tool SEV at different cutting widths (a) $\mu_c = 10^5$ N/m, (b) $\mu_c = 10^4$ N/m.

(22) can be found.

$$C_1 = \frac{\omega^- y_2^*(0) + y_2^{**}(0)}{2\Xi\Omega_n}, C_2 = \frac{\omega^+ y_2^{**}(0) - y_2^*(0)}{2\Xi\Omega_n} \quad (27)$$

The solution (25) shows that the SEV of tool-2 has four vibration modes. The first, second and the last two oscillation terms in the solution (25) denote respectively the effects of the cyclic oscillation of top wavy surface, the cyclic formation of shear bands and the coupled effects of the top wavy surface and the periodic shear bands on the tool-2 SEV. In terms of the results, the displacement-time curves of the tool-2 SEV motion can be obtained as shown in Fig. 22. The parameters used in the analysis are listed in Table 1. For simplicity, the phase angle differences are taken to be zero, $\theta_w = \theta_s = 0$. For comparison, the simulation results are also given in this figure, which shows a good agreement between these analytical and simulation results for both the low damping case and the high damping case. The influence generated by the relative damping on the stability of tool-2 SEV is evident. When it is sufficient large, the motion of tool-2 is stable. Otherwise, as the relative damping is small enough, the tool-2 SEV occurs and the resultant oscillation frequency of displacement is closer to that of the formation of shear bands. This implies that the tool-2 SEV process is governed by the shear banding instability behavior whereas the influence of wavy surface is not significant.

The additional cutting damping between the tool edge and adjacent flank face generates obvious influences on the stability of the tool-2 SEV cutting process. The displacement-time curves as shown in Fig. 23 illustrate that, when the additional cutting damping equals 10^5 N/m, the tool-2 SEV is stable if $w < 10$ μm . When $w > 50$ μm , the tool-2 SEV starts to go into unstable state (Fig. 23a). When the additional damping equals 10^4 N/m, the amplitude of tool-2 SEV increases sharply as the cutting width increases. As $w = 50$ μm , the unstable tool-2 SEV takes place (Fig. 23b). This SEV instability process is a typical phenomenon observed in the vibration cutting tests [46].

4.3. Analysis of tool-2 self-excited vibration stability

4.3.1. Stability conditions

As has been analyzed, the motion of the tool SEV becomes unstable once the relative damping is small enough or the cutting width is large enough. The method to verify the stability of tool SEV quantitatively is to analyze the stability boundary of vibration, which is also the critical occurrence condition of unstable vibration. According to the works of Wu and Liu [64], two types of stability boundary exist in the tool vibration cutting process. One is the lobed boundary which is the stability borderline of the tool vibration ascribed to the undulation of successive cut depth in turning. The other is tangent boundary which is the stability borderline tangential to the lobed instability regions. Generally, there are a series of tangent points between the two borderline curves. Evidently, at the concurrent tangent points, the tool SEV is in a critical equilibrium state. The energy dissipated in this state reaches a peak value relative to the adjacent states. When the chip depth changes in cutting, the maximum energy dissipation should be determined by the prescribed phase difference of two consecutive cutting processes.

With application of the analytical method of Wu and Liu [64], the stability limit of the tool-2 SEV can be determined. The cutting force in (15) is now rewritten as

$$F_y = -2w\tau_0(y_1 - y_2)[H_1 - H_2V + H_3(\dot{y}_2 - \dot{y}_1)] \quad (28)$$

where the dynamic cutting force coefficients are defined as

$$\begin{aligned} H_1 &= \frac{\sin\varphi[\cos 2(\varphi + \alpha - \beta) + 1]}{\sin^3 2(\varphi + \alpha - \beta)[\cot(2\varphi + \alpha - \beta) + 1]} \\ H_2 &= \frac{\varepsilon_m V \sin^2 \beta}{2 \cos \alpha} \frac{\cos^2(\alpha - \beta) + 2 \cos(\alpha - \beta) \cos(2\varphi + \alpha - \beta) + 1}{\sin^2 2(\varphi + \alpha - \beta)[\cos(\alpha - \beta) + \cos(2\varphi + \alpha - \beta)]^2} \\ H_3 &= -\frac{\cos \alpha \cos 2(\varphi + \alpha - \beta) + \cos \alpha + \varepsilon_m V \sin^2 \beta}{\cos \alpha \sin 2(\varphi + \alpha - \beta)} H_2 \end{aligned} \quad (29)$$

where α , β and φ are the rake angle, friction angle and the shear angle, respectively. The small quality ε_m is related to the mean friction coefficient at the tool-chip interface and can be determined from steady-state orthogonal cutting experiments.

From the simulation curves at small relevant damping in Fig. 22, we can assume that the tool-2 SEV complies with the oscillation regulation of sinusoidal function with given amplitude and phase angle. Assume the top wavy surface vibrates with the angular velocity ω_w and the amplitude of A_w , i.e., according to the relation (14). During the tool-2 SEV cutting, the oscillation amplitude of tool-2 SEV is assumed to have the same order in two continuous cutting processes. The tool-2 SEV is represented with the displacement-time relation $y_2(t)$ in (24). From the expressions of (14) and (24), the instantaneous cut thickness and its change rate of time can be written as

$$\begin{aligned} y_1 - y_2^{**} &= y_0 - \left(1 - \frac{A_{w0}}{\Psi_1} \cos \Theta_w\right) y_2^{**} - \frac{A_{w0}}{\Psi_1 \omega_w} \sin \Theta_w y_2^{**} \\ y_2^{**} - \dot{y}_1 &= \left(1 - \frac{A_{w0}}{\Psi_1} \cos \Theta_w\right) \dot{y}_2^{**} - \frac{\omega_w A_{w0}}{\Psi_1} \sin \Theta_w y_2^{**} \end{aligned} \quad (30)$$

From the cutting force in expressions (28) and (19), the energy function in a cutting cycle $[0, 2\pi]$ can be represented as:

$$E(\Theta_{\Pi_i}) = \int_0^{2\pi} \dot{E}(\Theta_{\Pi_i}; t) d\omega_w t = 2\tau_0 \omega \int_0^{2\pi} \left[\dot{y}_2^{**} [H_1 - H_2 + H_3(\dot{y}_2^{**} - \dot{y}_1)] \times (y_2^{**} - y_1) - \frac{\mu_c \omega}{V} \dot{y}_2^{**} \right] d\omega_w t \quad (31)$$

In (30) and (31), the contribution of the general homogeneous solution y_2^* in the complete solution (24) to the cutting energy is neglected since it goes to zero in the stable vibration process. Since we have known that the vibration sources of tool-2 SEV comes from the oscillation of the top wavy surface and the cyclic formation of shear bands, the first two terms with $i=1$ and 2 in (25) denote respectively the separating effect of the wavy surface and cyclic formation of shear banding on the tool-2 SEV and the last two terms with $i=3$ and 4 denote the coupled effects. When the tool-2 SEV motion reaches a critical state, the maximum energy will be dissipated by the system. Thus, the extreme condition

$$\frac{\partial E(\Theta_{\Pi_i})}{\partial \Theta_{\Pi_i}} = 0 (i = 1, \dots, 4) \quad (32)$$

gives the phase difference corresponding to the critical stable state of the Tool-2 SEV.

When the cutting speed is low enough and no multiple shear banding instability occurs, the tool-2 SEV motion is only related to the oscillation of the top wavy surface. At this time,

$$y_2^{**}(t) = \Psi_1 \sin(\omega_w t + \Theta_w) \quad (33)$$

By insetting (33) and (30) into (31), and using the condition (32), like Wu and Liu [64] did, the phase difference is found to satisfy the following equation

$$\tan \Theta_w = \frac{H_1 + H_2 V}{\omega_w y_0 H_3} \quad (34)$$

It can be seen that the function $\tan \Theta_w$ is related to the angular velocity ω_w , the mean cut depth y_0 and the cutting speed V . From the expressions of H_1, H_2 and H_3 in (29), its value is calculated as a large negative number. Thus, the phase difference is found as $\Theta_w = 2n\pi + 3\pi/2$ ($n=1, 2, \dots$). In terms of this results and the relations (30), the motion Eq. (15) is rewritten as

$$m_0 \ddot{y}_2^{**} + \left[\mu_0 - 2w\tau_0 \left(\frac{A_{w0}}{\Psi_1} \frac{H_1 - H_2 V}{\omega_w} - y_0 H_3 \right) + \frac{\mu_c \omega}{V} \right] \dot{y}_2^{**} + \left[k_0 + 2w\tau_0 \omega_w \left(\frac{H_1 - H_2 V}{\omega_w} + y_0 H_3 \frac{A_{w0}}{\Psi_1} \right) \right] y_2^{**} = 2w\tau_0 y_0 (H_1 - H_2 V) \quad (35)$$

where only the linear terms of the cutting force in (28) are considered. The stability of the tool-2 SEV depends on the total damping factor and the total stiffness factor

$$\Delta_\mu = \mu_0 - 2w\tau_0 \left(\frac{A_{w0}}{\Psi_1} \frac{H_1 - H_2 V}{\omega_w} - y_0 H_3 \right) + \frac{\mu_c \omega}{V}$$

$$\Delta_k = k_0 + 2w\tau_0 \left(H_1 - H_2 V + \omega_w y_0 H_3 \frac{A_{w0}}{\Psi_1} \right) \quad (36)$$

If $\Delta_\mu > 0$, the tool-2 SEV is stable. Otherwise, it becomes unstable and chatter occurs. This implies that the critical stability condition is given by $\Delta_\mu = 0$. Consequently, the critical width yields

$$w_{c1} = \frac{\mu_0}{2\tau_0 \left(\frac{A_{w0}}{\Psi_1} \frac{H_1 + H_2 V}{\omega_w} - y_0 H_3 \right) - \frac{\mu_c \omega}{V}} \quad (37)$$

This result is agreement with that of Wu and Liu [64] as $A_{w0} = \Psi_1$. When the cutting speed is high enough, the multiple shear banding instability occurs, which would generate influence on the tool-2 SEV. For clarity, the solution in (25) is taken as

$$y_2^{**}(t) = \Psi_2 \sin(\omega_s t + \Theta_s) \quad (38)$$

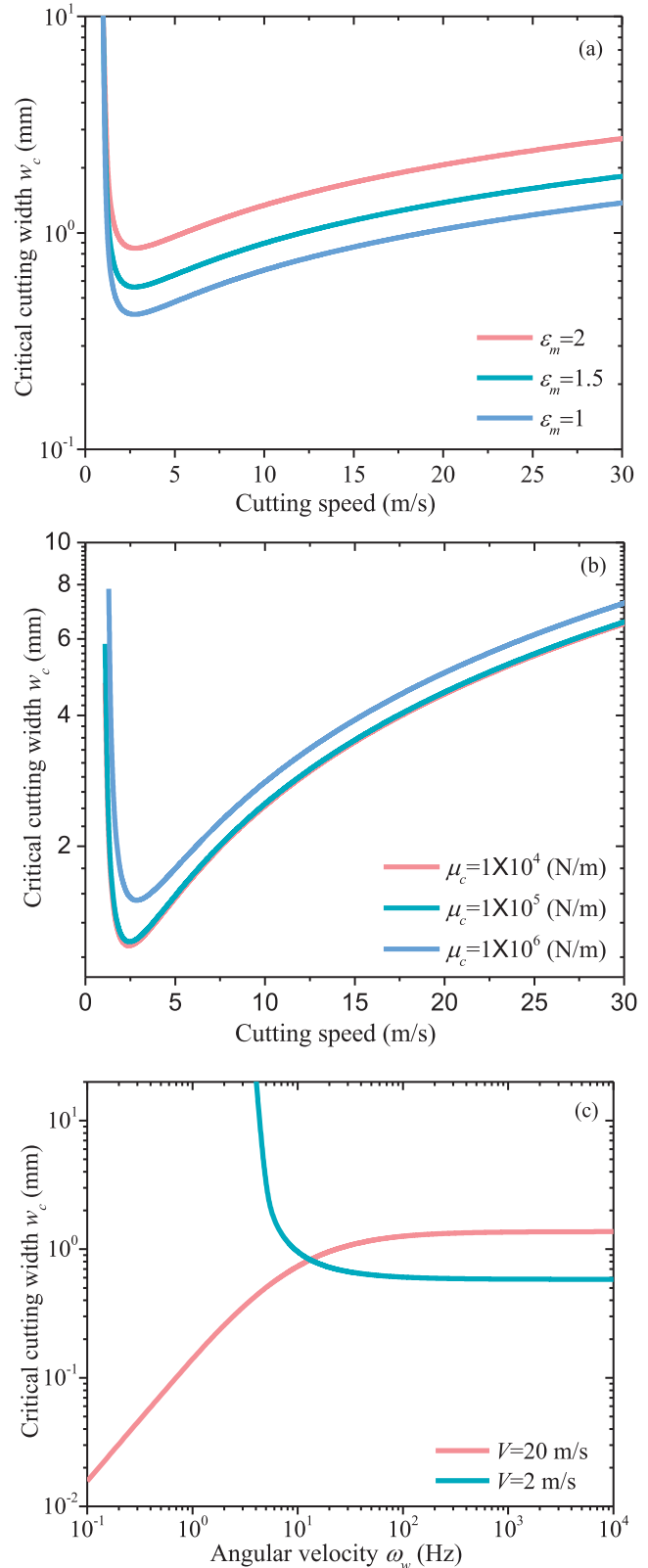


Fig. 24. The critical widths vary with the increasing cutting speed at different the exponential damping coefficient ϵ_m (a) and of the penetration damping resistance (b). The figure (c) shows the dependence of the critical width on the oscillation angular frequency of wavy surface at different cutting speeds.

Through the same analysis procedure above, we may obtain the equivalent phase angular corresponding to the critical stable state of the tool-2 SEV as $\Theta_s = 2n\pi + 3\pi/2$ ($n = 1, 2, \dots$). And the instantaneous cut thickness and its rate of time are rewritten as

$$y_1 - y_2^{**} = y_0 - \sqrt{2}A_{w0} \frac{1 - \eta^2}{\eta^3} - \frac{A_{w0}}{\eta^4 \omega_w \Psi_2} \left(\sin \Theta_s - \frac{1 - \eta^2}{\sqrt{2}} \cos \Theta_s \right) y_2^{**} + \left[\frac{A_{w0}}{\eta^3 \Psi_2} \left((1 - \eta^2) \sin \Theta_s + \frac{1}{\sqrt{2}} \cos \Theta_s \right) - 1 \right] y_2^{**}$$

$$\dot{y}_2^{**} - \dot{y}_1 = \omega_w A_{w0} \frac{1 - \eta^2}{\eta^2} + \left(1 - \frac{A_{w0}}{\eta^3 \Psi_2} \cos \Theta_s \right) \dot{y}_2^{**} - \frac{\omega_w A_{w0}}{\eta^2 \Psi_2} \sin \Theta_s y_2^{**} \quad (39)$$

where $\eta = \omega_s / \omega_w$ is the frequency ratio. By using this result, the motion equation of tool-2 SEV (15) becomes

$$m_0 \ddot{y}_2^{**} + \left\{ \mu_0 - \left[2\omega\tau H_3 \left(y_0 - \sqrt{2} \frac{1 - \eta^2}{\eta^3} A_{w0} \right) \left(\frac{A_{w0} \cos \Theta_s}{\Psi_2 \eta^3} - 1 \right) - \frac{2\omega\tau A_{w0}}{\eta \omega_w \Psi_2} \left(H_1 + H_2 V + \omega_w A_{w0} H_3 \frac{\eta^2 - 1}{\eta^2} \right) \times \left(\frac{1}{\eta^3} \sin \Theta_s - \frac{1 - \eta^2}{\sqrt{2} \eta^3} \cos \Theta_s \right) - \frac{\mu_c w}{V} \right] \right\} \ddot{y}_2^{**} + \left\{ k_0 - 2\omega\tau \left[\left(H_1 + H_2 V - \omega_w A_{w0} H_3 \frac{1 - \eta^2}{\eta^2} \right) \times \left[\frac{A_{w0}}{\Psi_2} \left(\frac{1 - \eta^2}{\eta^3} \sin \Theta_s + \frac{1}{\sqrt{2} \eta^3} \cos \Theta_s \right) \right] + \frac{\omega_w A_{w0} H_3 \sin \Theta_s}{\eta^2 \Psi_2} \left(y_0 - \sqrt{2} \frac{1 - \eta^2}{\eta^3} A_{w0} \right) \right] \right\} \dot{y}_2^{**} = 2\omega\tau \left(y_0 - \sqrt{2} \frac{1 - \eta^2}{\eta^3} A_{w0} \right) \left(H_1 + H_2 V - \omega_w A_{w0} H_3 \frac{1 - \eta^2}{\eta^2} \right) \quad (40)$$

$$w_{c3} = \frac{-\eta_3^4 \mu_0}{\frac{2\tau A_{w0}}{\Psi_3} \left(\frac{H_1 - H_2 V}{\omega_w} + \frac{1 - \eta_3^2}{\eta_3^2} A_{w0} H_3 \right) \left(\cos \Theta_{\Pi_3} + \frac{1 - \eta_3^2}{\sqrt{2}} \sin \Theta_{\Pi_3} \right) + 2\tau y_0 H_3 \left(1 - \sqrt{2} \frac{A_{w0}}{y_0} \frac{1 - \eta_3^2}{\eta_3^3} \right) \left(1 + \frac{A_{w0}}{\Psi_3} \frac{\sin \Theta_{\Pi_3}}{\eta_3^3} \right) - \frac{\eta_3^4 \mu_c}{V}} \quad (45-1)$$

and

$$w_{c4} = \frac{\eta_4^4 \mu_0}{\frac{2\tau A_{w0}}{\Psi_4} \left(\frac{H_1 - H_2 V}{\omega_w} + \frac{1 - \eta_4^2}{\eta_4^2} A_{w0} H_3 \right) \left(\cos \Theta_{\Pi_4} + \frac{1 - \eta_4^2}{\sqrt{2}} \sin \Theta_{\Pi_4} \right) + 2\tau y_0 H_3 \left(1 - \sqrt{2} \frac{A_{w0}}{y_0} \frac{1 - \eta_4^2}{\eta_4^3} \right) \left(1 - \frac{A_{w0}}{\Psi_4} \frac{\sin \Theta_{\Pi_4}}{\eta_4^3} \right) - \frac{\eta_4^4 \mu_c}{V}} \quad (45-2)$$

Similarly, based on the condition of total damping coefficient to be zero, the critical cutting width is given by

$$w_{c2} = \frac{\eta^6 \mu_0}{2\tau A_{w0} H_3 \left[\frac{\eta^3 y_0}{A_{w0}} - \sqrt{2}(1 - \eta^2) \right] \left(\frac{A_{w0} \cos \Theta_s}{\Psi_2} - \eta^3 \right) - 2\tau \frac{A_{w0}^2}{\Psi_2} \left[\frac{\eta^2 (H_1 - H_2 V)}{\omega_w A_{w0}} - H_3 (\eta^2 - 1) \right] \left(\sin \Theta_s - \frac{1 - \eta^2}{\sqrt{2}} \cos \Theta_s \right) - \frac{\eta^6 \mu_c}{V}} \quad (41)$$

We can see that this result is identical with that in (37) as $\eta = 1$ and $\Theta_s = 2n\pi + 3\pi/2$.

For studying the coupled effects of the top wavy surface and the periodic formation of shear bands on the tool-2 SEV process, we need to inspect the last two terms of solution (25). At this time, we have

$$y_2^{**}(t) = (-1)^{i+1} \Psi_{i+2} \cos(\omega_{\Pi_{i+2}} t + \Theta_{\Pi_{i+2}}), \quad (i = 1, 2) \quad (42)$$

Setting $\eta_{i+2} = \omega_{\Pi_{i+2}} / \omega_w$ ($i = 1, 2$), then the instantaneous cut thickness and its rate of time is represented as

$$y_1 - y_2^{**} = \left(y_0 - \sqrt{2} A_{w0} \frac{1 - \eta_{i+2}^2}{\eta_{i+2}^3} \right) + \frac{(-1)^i A_{w0}}{\eta_{i+2}^4 \omega_w \Psi_{i+2}} \times \left(\cos \Theta_{\Pi_{i+2}} + \frac{1 - \eta_{i+2}^2}{\sqrt{2}} \cos \Theta_{\Pi_{i+2}} \right) y_2^{**}$$

$$+ \left[\frac{(-1)^j A_{w0}}{\eta_{i+2}^3 \Psi_{i+2}} \left(\sin \Theta_{\Pi_{i+2}} - \frac{1 - \eta_{i+2}^2}{\sqrt{2}} \cos \Theta_{\Pi_{i+2}} \right) - 1 \right] y_2^{**}$$

$$\dot{y}_2^{**} - \dot{y}_1 = \left(1 - \frac{(-1)^i A_{w0}}{\eta_{i+2}^3 \omega_w \Psi_{i+2}} \sin \Theta_{\Pi_{i+2}} \right) \dot{y}_2^{**} - \frac{(-1)^{i+1} A_{w0}}{\eta_{i+2}^2 \Psi_{i+2}} \cos \Theta_{\Pi_{i+2}} y_2^{**} - \frac{\eta_{i+2}^2 - 1}{\eta_{i+2}^2} A_{w0} \quad (43)$$

The motion equation of tool-2 SEV (15) is given as

$$m_0 \ddot{y}_2^{**} + \mu_0 \dot{y}_2^{**} + k_0 y_2^{**} = 2\omega\tau \left(y_0 - \sqrt{2} A_{w0} \frac{1 - \eta_{i+2}^2}{\eta_{i+2}^3} \right) \left(H_1 - H_2 V - \frac{\eta_{i+2}^2 - 1}{\eta_{i+2}^2} A_{w0} H_3 \right) + w \left[2\tau H_3 \left(y_0 - \sqrt{2} A_{w0} \frac{1 - \eta_{i+2}^2}{\eta_{i+2}^3} \right) \left(1 - \frac{(-1)^i A_{w0}}{\eta_{i+2}^3 \omega_w \Psi_{i+2}} \sin \Theta_{\Pi_{i+2}} \right) + 2\tau \frac{(-1)^j A_{w0}}{\eta_{i+2}^4 \omega_w \Psi_{i+2}} \left(H_1 - H_2 V - \frac{\eta_{i+2}^2 - 1}{\eta_{i+2}^2} A_{w0} H_3 \right) \times \left(\cos \Theta_{\Pi_{i+2}} + \frac{1 - \eta_{i+2}^2}{\sqrt{2}} \sin \Theta_{\Pi_{i+2}} \right) - \frac{\mu_c}{V} \right] \dot{y}_2^{**} + 2\omega\tau \left[\left(H_1 - H_2 V - \frac{\eta_{i+2}^2 - 1}{\eta_{i+2}^2} A_{w0} H_3 \right) \times \left[\frac{(-1)^i A_{w0}}{\eta_{i+2}^3 \Psi_{i+2}} \left(\sin \Theta_{\Pi_{i+2}} - \frac{1 - \eta_{i+2}^2}{\sqrt{2}} \cos \Theta_{\Pi_{i+2}} \right) - 1 \right] - \left(y_0 - \sqrt{2} A_{w0} \frac{1 - \eta_{i+2}^2}{\eta_{i+2}^3} \right) \frac{(-1)^{i+1} A_{w0} H_3}{\eta_{i+2}^2 \Psi_{i+2}} \right] y_2^{**} \quad (44)$$

Thus, by neglecting the nonlinear terms in (44), we obtain the critical width as follows:

In (45), $\eta_3 = 1 - \eta \leq 1$ and $\eta_4 = 1 + \eta \geq 1$ corresponds to two different modes, w_{c3} and w_{c4} , which reflect respectively the coupling effects on the tool-2 SEV cutting process in different frequency ratios.

4.3.2. Results and discussion

Fig. 24a and b show the predicted stability limits of the tool-2 SEV from the result in (37). It shows that, only when the oscillation of wavy surface presents, the critical cutting width increases proportionally to the cutting speed in high-speed cutting process approximately. As cutting speed approaches to zero, the stability limit increases sharply and the minimum cutting width corresponding to a particular low cutting speed presents. This indicates that the tool-2 SEV cutting process with low cutting speed is a stability cutting process. Furthermore, the critical width is sensitive to the exponential damping coefficient ϵ_m of the mean friction coefficient at the tool-chip face in a wide range of cutting speed Fig. 24a). This parameter is related to the dynamic cutting force coefficients in ((29) through the velocity-dependent friction property and

a larger ε_m in value will result in smaller cutting force. Thus, this result also reveals the influences of cutting forces on the critical cutting width. That is to say, diminishing of the cutting forces due to the rise of ε_m increases the damping resistance at the tool-chip face and further increases the stability of the tool-2 SEV ($\varepsilon_m = 2$). The effect of the penetration damping resistance μ_c in the tool nose region on the stability limit is illustrated in Fig. 24b. This effect is significant in low-speed cutting process and there is no evident change in high-speed cutting. Since the coefficient increases with the tool edge radius increasing, the larger μ_c in value will produce a larger penetration damping resistance which results in a more stable motion for the tool-2 SEV.

Fig. 24c illustrates the dependence of the critical width on the oscillation angular frequency of wavy surface. For cutting speed 20 m/s, the serrated chip forms. The critical width increases sharply with increasing the angular frequency before 100 Hz and then remains constant thereafter. At this time, the tool-2 SEV motion goes into a stable state induced by the multiple shear banding instability and is almost irrelevant to the periodic changing chip thickness. In the low-speed cutting process with the cutting speed 2 m/s, the continuous chip forms. When the angular frequency is less than 10 Hz, the stability curve rises sharply hyperbolically with a decrease of the angular frequency, which indicates that the tool-2 SEV motion is always stable. It's worth noting that the total stiffness factor reaches the maximum when the angular velocity equals zero (see (36) $H_3 < 0$). When the angular velocity is larger than 200 Hz, the critical width remains constant, implying that the high-frequency oscillation of machined wavy surface doesn't affect the tool-2 SEV. Similarly, the total stiffness factor reaches the minimum when the angular velocity reaches maximum. In the frequency range of 10–200 Hz, the wavy surface oscillation yields a significant influence on the critical width. These curves of critical width in Fig. 24 is a typical stability boundary observed in a large number of machining experiments [46].

It is clear that the ratio of angular velocity $\eta = \omega_s / \omega_w$ in (41) presents in high power form and thus it may generate a significant influence on the stability limit of the tool-2 SEV. The condition $\eta = 0$ may be considered in two cases. 1) the condition $\omega_s = 0$ and $\omega_w \neq 0$ means no periodic shear banding instability occurs in chip, i.e. the continuous chip with various chip thickness develops in low-speed cutting process. At this point, the SEV of tool does not occur; 2) the condition $\omega_s \neq 0$ and $\omega_w \rightarrow \infty$ denotes that the SEV cutting process has a high oscillation frequency of wavy machined surface, which makes various chip thickness become constant chip thickness, and thus the serrated chip with uniform morphology forms in the SEV cutting (see Fig. 16d-f). When $\eta > 0$, the periodic shear banding formation produces evident influence on the stability limit of the tool-2 SEV, as illustrated by the curves in Fig. 25a. These curves denote the variation of the critical width with the increasing cutting speed is dependent on the frequency ratios η . The condition $\eta = 1$, i.e. $\omega_s = \omega_w$ indicates that the influences on the tool-2 SEV generated by the periodic shear banding formation and by the wavy machined surface oscillation are exactly the same. The condition $\eta > 1$, i.e. $\omega_s > \omega_w$ shows that both the frequency of shear banding formation and the frequency of the wavy surface oscillation are certainly in the low-frequency domain. Thus the serrated chip formation makes the stability of the tool-2 SEV decrease obviously. The condition $\eta < 1$, i.e. $\omega_s < \omega_w$ denotes, on the one hand, that the frequency of the wavy surface oscillation is larger than and close to the frequency of shear banding formation. The serrated chip with ununiformed morphology forms and the tool-2 SEV is unstable. On the other hand, it denotes that the frequency of the wavy surface oscillation is quite high and the serrated chip with ununiformed morphology develops and the tool-2 SEV is unstable. But, the stability of the SEV process increases sharply. For the case of low-speed cutting process and the oscillation frequency of wavy surface with 120 kHz, no shear banding formation occurs and continuous chip develops. The wavy surface oscillation with long wave length induces extremely weak SEV for the tool-2 so that the tool-2 SEV stability increases evidently. When the serrated chip forms in the high-speed cutting process, the frequency of shear banding instability increases proportionally to the cutting speed

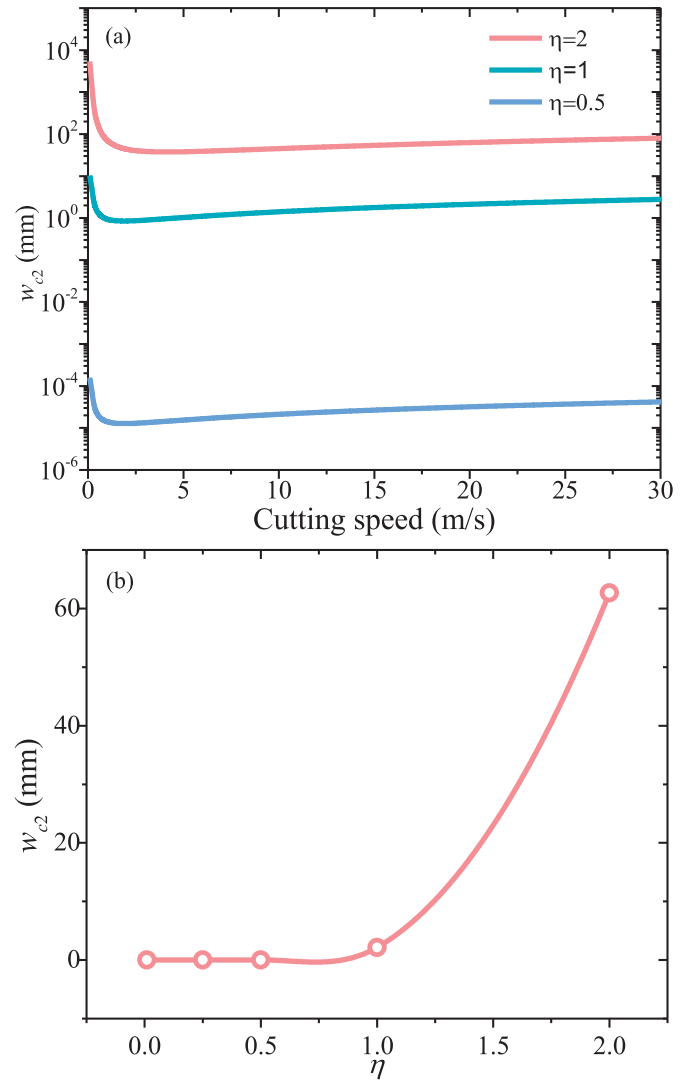


Fig. 25. The critical widths vary with the increasing cutting speed at different frequency ratio (a) and with the frequency ratio (b).

Fig. 6). The stability of tool-2 SEV depends upon the shear banding instability frequency and the cutting speed. In terms of the extreme condition of energy (32) and the critical width in (41), the stability curve of tool-2 SEV within the limited range of frequency ratio from 0 to 2 is obtained as shown in Fig. 25b. Comparing with the frequency of periodic shear banding formation that is in the order of 2×10^2 kHz, the higher frequency of wavy surface results in the stability decreasing of the tool-2 SEV cutting process, while the lower frequency of wavy surface in its stability increasing.

The curves in Fig. 26 represent the evolution of the critical widths w_{c3} and w_{c4} with the increasing cutting speed. When the continuous chip forms in the low-speed cutting process, the multiple shear banding instability does not occur for the plastic flow of chip material. As well known that, at this time, the effect of the wavy cut thickness on SEV cutting is not significant. Therefore, the coupled effects on the cutting process almost disappear which results in evident increase of the stability of tool-2 SEV. When the cutting speed increases, the serrated chip forms. The influence of coupled effects on SEV cutting becomes significant due to the occurrence of the periodic shear banding instability. In the high-speed cutting process, the influence of the multiple shear banding instability in the serrated chip prevail over that of the changing cut

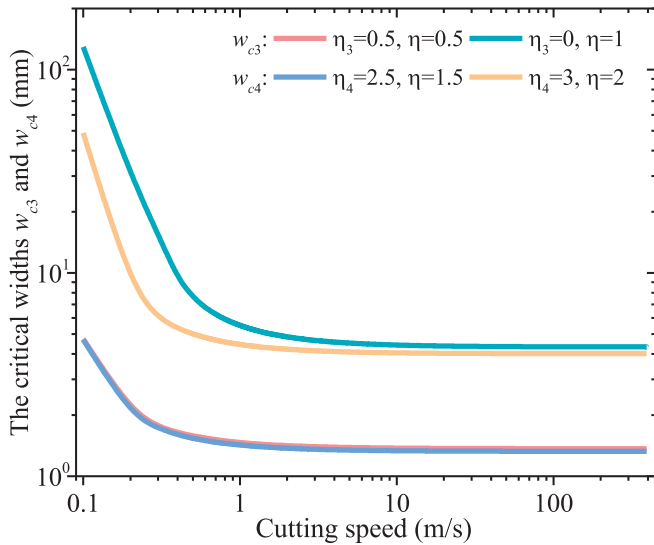


Fig. 26. The variations of the critical widths w_{c3} and w_{c4} with the cutting speed increasing at different frequency ratio.

Table 2

The parameters used in the present analysis [13].

Name(Unit)	Symbol	Value
Mass (Kg)	m_0	0.36
Damping (N s/m)	μ_0	0.001, 0.25
Damping coefficient (N/m)	μ_c	$10^4, 10^5, 10^6$
Cutting speed (m/s)	V	20
System stiffness (N/m)	k_0	4000
Width of cutting (μm)	w	1, 10, 100
Friction angle (rad)	β	0.12
Shear angle (rad)	φ	$\pi/4$
Cutting thickness (μm)	y_0	100
Amplitude (μm)	A_w	10
Wave surface frequency (kHz)	ω_w	100–3000
Shear stress (Pa)	τ_0	0.37×10^8
Amplitude of shear stress (Pa)	A_s	$0.3\tau_0$
Shear band frequency (kHz)	ω_s	240
Wave surface phase angle (rad)	θ_w	–
Shear band phase angle (rad)	θ_s	–

thickness and rises the stability of the tool-2, so that the critical widths are almost unchanged as the cutting speed increases.

From the displacement expression (25), we can see that the last two terms in (25) describe the coupled effects of the changing cut thickness and periodic shear banding instability in the SEV cutting process in two different modes. One mode is w_{c3} with $\eta_3 = 1 - \eta = 1 - \omega_s/\omega_w < 1$ in (45–1) and the other is w_{c4} with $\eta_4 = 1 + \eta = 1 + \omega_s/\omega_w > 1$ in (45–2). Evidently, the two modes are symmetric about $\eta=0$ or $\eta_3 = \eta_4 = 1$. In this case, $\omega_s = 0$ and the extreme condition (32) gives the $\Theta_{\Pi3} = \Theta_{\Pi4} = 2n\pi$. From the critical widths in (45), it is easily to obtain $w_{c3} + w_{c4} = 0$, i.e., the coupled effects from the two modes on tool-2 SEV offset each other. For $\eta_3 < 1$ and $\eta_4 > 1$, the equivalent phase differences for the two modes can be determined as $\eta = 2$, $\Theta_{\Pi3} = -\Theta_{\Pi4} \approx (2n+1)\pi$, $\eta = 1$, $\Theta_{\Pi3} = \Theta_{\Pi4} \approx n\pi$, $\eta = 0.5, 1.5$, $\Theta_{\Pi3} = -\Theta_{\Pi4} \approx (2n+1/2)\pi$ in terms of the energy function (31) and the extreme condition of energy (32). The symmetric nature of the coupled effects on tool-2 SEV is represented by the ratio η of the instability frequency of multiple shear bands to oscillation frequency of the undulatory cut thickness. As $\eta < 1$, the vibration mode w_{c3} dominates the coupled effect. Since the shear banding instability frequency is independent of the oscillation frequency of the changing cut thickness (see Fig. 16), $\eta = 0.5$ means $\omega_w = 2\omega_s$. The high-frequency oscillation generated by the changing cut thickness reduces the coupled effect so that the stability of tool-2 SEV increases obviously as shown by the

curve with $\eta = 0.5$ in Fig. 26. In addition, $\eta = 1$ or $\omega_w = \omega_s$ corresponds to the resonance between the periodic shear banding instability and the oscillation of changing cut thickness. Thus, the stability of the tool-2 SEV decreases sharply (the curve with $\eta = 1$ in Fig. 26). As $\eta > 1$ the vibration mode w_{c4} governs the coupled effect. The condition $\eta = 1.5$ or $\omega_s = 1.5\omega_w$ indicates that the SEV cutting process is certainly under a low-frequency state in terms of the results in Fig. 15. Therefore, SEV is in a more stable state when $\eta = 1.5$ as shown in Fig. 26. As the oscillation frequency of the changing cut thickness decreases continuously until $\eta = 2$ or $\omega_s = 2\omega_w$, the contribution of the changing cut thickness to the coupled effect almost disappears. The periodic shear banding instability becomes the dominating factor in the coupled effect, which decreases greatly the tool-2 SEV stability (the curve with $\eta = 2$ in Fig. 26). It should be noted that the curve with $\eta = 2$ is close to the resonance curve with $\eta = 1$. This is because that the resonance frequency is the instability frequency of the periodic shear bands as demonstrated by the simulation and analytical results in Fig. 17 and Fig. 21.

5. Conclusions

In conclusion, metal cutting process with vibration is intrinsically complex physical phenomena, in which the tool in vibration and the chip material in plastic flow can be treated as a coupled thermodynamic system. The study of this process proposes new challenges on the analyzing, modelling and experimental methods. In this work, the CEL FE model with natural advantage is used to perform the numerical simulations of the high-speed cutting process with two types of tool vibration. The theoretical models are also established and show good agreement with simulation results. Several key manufacturing issues are analyzed, and major findings are summarized as below:

- The numerical simulations on the cutting process demonstrate that the low-frequency FV promotes the formation of serration chip, and the resonance yields the strongest impacting on the chip shape and the cutting force. When the tool frequency increases, the tool vibration may hinder the evolution of shear bands, which results in the transition of the serrated chip into the continuous chip. Since the critical FV frequency is unattainable in industrial applications, vibration assisted machining may worsen the negative effect of shear banding in the high-speed cutting process. The high-frequency vibration can be considered as a possible strategy to suppress the occurrence of shear banding instability in the serrated chip.
- The linear stability analysis on the FV cutting process gives the interpretation on the mechanisms of the formation of serrated chip and the transition of chip shape. The high-frequency oscillation of shear stress doesn't change the formation mechanism of the multiple shear bands and the shear banding instability frequency in the high-speed cutting process, but makes the distribution of shear deformation energy of material within shear bands tend to be homogenous. The high-frequency oscillation of pressure on the rake face is the key cause for the transition of chip shape. The pressure oscillation dissipates the partial work done by tool which is necessary for the shear localized deformation of chip material in the PSZ. Thus, it reduces the thermal softening effect of chip material deformation and results in the chip transition of continuous from serrated.
- A double-tool FE model is used for the simulation of the SEV cutting process. The numerical results reveal that the wavy cutting depth strongly affects the cutting process. The low-frequency oscillation of the cut depth causes evident variations of the cutting force in amplitude which produce the serrated chip with non-uniform serrations. The influence of the high-frequency oscillation of the cut depth on the cutting force is slight, therefore, the multiple shear banding instability governs the serrated chip development with uniform serrations.

- (iv) The stability of SEV in cutting process depends on the friction damping coefficient at the rack face, the penetration damping resistance, the ratio of the oscillation frequency of top wavy surface and the instability frequency of the multiple shear banding and their coupling effects. In the high-speed cutting process with SEV, increasing damping resistances and the frequency ratios result in higher stability limit for the tool-2 motion. The coupling effects of the top wavy surface and the multiple shear banding instability are limited in the low-speed cutting process. In this cases, two oscillation modes determine the effects on the tool SEV motion respectively. Occurrence of shear bands sharpening decrease the stability of SEV.

Table 2.

Acknowledgments

This work was supported by the National Nature Science Foundation of China (Grant numbers 51575029, 11572337, 11772346).

References

- Taylor FW. On the art of cutting metals. *Trans ASME* 1907;28:31–350.
- Zhang J, Cui T, Ge C, Sui Y, Yang H. Review of micro/nano machining by utilizing elliptical vibration cutting. *Intern J Mach Tools Manuf* 2016;106:109–26.
- Quintana Guillem, Ciurana Joaquim. Chatter in machining processes: A review. *Intern J Mach Tools Manuf* 2011;51:363–76.
- Siddhpura M, Paurobally R. A review of chatter vibration research in turning. *Intern J Mach Tools Manuf* 2012;61:27–47.
- Arnold RN. The mechanism of tool vibration in the cutting of steel. *Proc Instn Mech Eng* 1946;154:261–84.
- Tobias SA. Machine tools vibrations. Spain: URMO; 1961.
- Xiao M, Sato K, Karube S, Soutome T. The effect of tool nose radius in ultrasonic vibration cutting of hard metal. *Intern J Mach Tools Manuf* 2003;43:1375–82.
- Shamoto E, Suzuki N, Hino R. Analysis of 3D elliptical vibration cutting with thin shear plane model. *CIRP Ann - Manuf Technol* 2008;57:57–60.
- Zhou M, Eow YT, Ngoi BK, Lim EN. Vibration-assisted precision machining of steel with PCD tools. *Mater Manuf Process* 2003;18:825–34.
- Zhou M, Ngoi BKA, Yusoff MN, Wang XJ. Tool wear and surface finish in diamond cutting of optical glass. *J Mater Process Technol* 2006;174:29–33.
- Xiao M, Karube S, Soutome T, Sato K. Analysis of chatter suppression in vibration cutting. *Intern J Mach Tools Manuf* 2002;42:1677–85.
- Moriwaki T, Shamoto E. Ultraprecision diamond turning of stainless steel by applying ultrasonic vibration. *CIRP Ann-Manuf Technol* 1991;40:559–62.
- Miguélez MH, Soldani X, Molinari A. Analysis of adiabatic shear banding in orthogonal cutting of Ti alloy. *Int J Mech Sci* 2013;75:212–22.
- Babitsky VI, Mitrofanov AV, Silberschmidt VV. Ultrasonically assisted turning of aviation materials: simulations and experimental study. *Ultrasonics* 2004;42:81–6.
- Liu K, Li XP, Rahman M. Characteristics of ultrasonic vibration-assisted ductile mode cutting of tungsten carbide. *Int J Adv Manuf Technol* 2008;35:833–41.
- Kumabe J, Fuchizawa K, Soutome T, Nishimoto Y. Ultrasonic superposition vibration cutting of ceramics. *Precis Eng* 1989;11:71–7.
- Adnan AS, Subbiah S. Experimental investigation of transverse vibration-assisted orthogonal cutting of AL-2024. *Int J Mach Tools Manuf* 2010;50(3):294–302.
- Sui H, et al. Feasibility study of high-speed ultrasonic vibration cutting titanium alloy. *J Mater Process Technol* 2017;247:111–20.
- E. Shamoto, N. Suzuki, *Ultrasonic vibration diamond cutting and ultrasonic elliptical vibration Cutting, comprehensive materials processing, Elsevier Limited 2015: 405–454.*
- Shamoto E, Moriwaki T. Ultraprecision diamond cutting of hardened steel by applying elliptical vibration cutting. *CIRP Ann - Manuf Technol* 1999;48:441–4.
- Suzuki N, Masuda S, Shamoto E. Ultraprecision machining of sintered tungsten carbide by applying ultrasonic elliptical vibration cutting. In: *Proceedings of 4th Euspen International Conference, Glasgow, Scotland 2004:187–8.*
- Nath C, Rahman M, Neo KS. A study on the effect of tool nose radius in ultrasonic elliptical vibration cutting of tungsten carbide. *J Mater Process Technol* 2009;209:5830–6.
- Kim GD, Loh BG. Characteristics of chip formation in micro V-grooving using elliptical vibration cutting. *J Micromech Microeng* 2007;17:1458–66.
- Suzuki N, Yokoi H, Shamoto E. Micro/nano sculpturing of hardened steel by controlling vibration amplitude in elliptical vibration cutting. *Precis Eng* 2011;35:44–50.
- Zhang X, et al. An analytical force model for orthogonal elliptical vibration cutting technique. *J Manuf Processes* 2012;14(3):378–87.
- Ahn JH, Lim HS, Son SM. Improvement of micromachining accuracy by 2-Dimensional vibration cutting. In: *Proceedings of the 14th Annual Meeting of the ASPE Monterey, 20; 1999. p. 150–3.*
- Kim GD, Loh BG. Machining of micro-channels and pyramid patterns using elliptical vibration cutting. *Int J Adv Manuf Technol* 2010;49:961–8.
- Kim GD, Loh BG. Characteristics of chip formation in micro V-grooving using elliptical vibration cutting. *J Micromech Microeng* 2007;17:1458–66.
- Kim GD, Loh BG. An ultrasonic elliptical vibration cutting device for micro V-groove machining: kinematical analysis and micro V-groove machining characteristics. *J Mater Process Technol* 2007;190:181–8.
- Brehl DE, Dow TA. Review of vibration-assisted machining. *Precis Eng* 2008;32:153–72.
- Brehl DE, Dow TA, Garrard K, Sohn A. Microstructure fabrication using elliptical vibration-assisted machining. In: *Proceedings of the 21th Annual Meeting of the ASPE, Monterey, 39; 2006. p. 511–14.*
- Brocato B, Dow TA, Sohn A. Micro-machining using elliptical vibration assisted machining. In: *Proceedings of the 19th Annual Meeting of the ASPE, Orlando, 34; 2004. p. 80–3.*
- Wiercigroch M, Krivtsov AM. Frictional chatter in orthogonal metal cutting. *Philosoph Trans Math Phys Eng Sci (Series A)* 2001;359:713–38.
- Wiercigroch M, Budak E. Sources of nonlinearities, chatter generation and suppression in metal cutting. *Philosoph Trans Math Phys Eng Sci* 2001;359:663–93.
- Stusty J, Polacek M. The stability of machine tools against self-excited vibrations in machining. *Intern Res Product Eng* 1963:465–74.
- Foulds LR, Neumann K. A network flow model of group technology. *Math Comput Model* 2003;38(5-6):623–35 9.
- Faassen RPH, van de Wouw N, Oosterling JAJ, Nijmeijer H. Prediction of regenerative chatter by modelling and analysis of high-speed milling. *Int J Mach Tools Manuf* 2003;43(14):1437–46 11.
- Das M, Tobias S. The relation between the static and the dynamic cutting of metals. *Intern J Mach Tool Design Res* 1967;7:63–89.
- Knight W. Application of the universal machinability chart to the prediction of machine–tool stability. *Intern J Mach Tool Design Res* 1968;8:1–14.
- Faassen RPH, van de Wouw N, Oosterling JAJ, Nijmeijer H. Prediction of regenerative chatter by modelling and analysis of high-speed milling. *Int J Mach Tools Manuf* 2003;43(14):1437–46.
- Tobias SA, Fishwick W. The chatter of lathe tools under orthogonal cutting conditions. *Trans ASME* 1958;80:1079–88.
- Stusty J, Polacek M. The stability of machine tools against self-excited vibrations in machining. In: *Proceedings of the International Research in Production Engineering Conference; 1963. p. 465–74.*
- Meritt JHE. Theory of self-excited machine–tool chatter. *Trans ASME J Eng Indust* 1965;87:447–54.
- Stusty J. Analysis of the state of research in cutting dynamics. *Annals CIRP* 1978;27:583–9.
- Mahnama M, Movahhedy MR. Prediction of machining chatter based on FEM simulation of chip formation under dynamic conditions. *Int J Mach Tools Manuf* 2010;50(7):611–20.
- Moufki A, Devillez A, Segreti M, Dudzinski D. A semi-analytical model of non-linear vibrations in orthogonal cutting and experimental validation. *Intern J Mach Tools Manuf* 2006;46:436–49.
- Turkes E, Orak S, Neseli S, Yaldiz S. Linear analysis of chatter vibration and stability for orthogonal cutting in turning. *Int J Refract Metals Hard Mater* 2011;29:163–9.
- Kim JS, Lee BH. An analytical model of dynamic cutting forces in chatter vibration. *Intern J Mach Tools Manuf* 1991;31:371–81.
- Gao Y, Suna R, Leopold J. Analysis of cutting stability in vibration assisted machining using an analytical predictive force model. In: *15th CIRP Conference on Modelling of Machining Operations Procedia CIRP*, 31; 2015. p. 515–20.
- Vela-Martínez L, Jáuregui-Correa JC, González-Brambila OM, Herrera-Ruiz G, Lozano-Guzmán A. Instability conditions due to structural nonlinearities in regenerative chatter. *Nonlinear Dyn* 2009;56:415–27.
- Shuang Fei, Chen Xiangyu, Ma Wei. Numerical analysis of chip formation mechanisms in orthogonal cutting of Ti6Al4V alloy based on a CEL model. *Int J Mater Form. January 2017. doi:10.1007/s12289-017-1341-z.*
- Ma W, Chen X, Shuang F. The chip-flow behaviors and formation mechanisms in the orthogonal cutting process of Ti6Al4V alloy. *J Mech Phys Solids* 2017;98:245–70.
- Ye GG, Xue SF, Ma W, Dai LH. Onset and evolution of discontinuously segmented chip flow in ultra-high-speed cutting Ti-6Al-4V. *Int J Adv Manuf Technol* 2016. doi:10.1007/s00170-016-8847-2.
- Molinari A, Soldani X, Miguélez MH. Adiabatic shear banding and scaling laws in chip formation with application to cutting of Ti-6Al-4V. *J Mech Phys Solids* 2013;61:2331–59.
- Hortig C, Svendsen B. Simulation of chip formation during high-speed cutting. *J Mater Process Technol* 2007;186:66.
- Al-Athel KS, Gadala MS. The use of volume of solid (VOS) approach in simulating metal cutting with chamfered and blunt tools. *Int J Mech Sci* 2011;53:23–30.
- Kim KW, Sin H-C. Development of a thermo-viscoplastic cutting model using finite element method. *Int J Mach Tools Manuf* 1996;36:379–97.
- Ozel T, Altan T. Determination of workpiece flow stress and friction at the chip-tool contact for high-speed cutting. *Int J Mach Tools Manuf* 2000;40:133–52.
- Lee S, Lin CF. High-temperature deformation behavior of Ti6Al4V alloy evaluated by high strain-rate compression tests. *J Mater Process Technol* 1998;75:127–36.
- Chen X, Shuang F, Ma W. Numerical simulation of metal vibration cutting. In: *Proceeding of the 12th National Academic Conference on the Impacting Dynamics, Oct. 21-25, 2015, 138-141, 36. Also, Transaction of Beijing Institute of Technology; 2016. p. 199-203. (In Chinese).*
- Molinari A. Collective behavior and spacing of adiabatic shear bands. *J Mech Phys Solids* 1997;45:1551–75.
- Bai YL. Thermo-plastic instability in simple shear. *J Mech Phys Solids* 1982;36:195–207.

- [63] Burns TJ, Davies MA. Nonlinear dynamics model for chip segmentation in machining. *Phys Rev Lett* 1997;79:447–50.
- [64] Wu DW, Liu CR. An analytical model of cutting dynamics. Part 2 Verification. *Trans ASME J Eng Ind* 1985;107:112–18.
- [65] Kudinov VA, et al. Experimental investigation of the nonlinearity of the dynamic characteristic of the cutting process. Translated by M. M. Barash. *Stanki I Instrument* 1978;49:11–13.